nature communications

Article

https://doi.org/10.1038/s41467-024-51389-4

A population of Insula neurons encodes for social preference only after acute social isolation in mice

Received: 20 December 2022

Accepted: 5 August 2024

Published online: 21 August 2024

Check for updates

Christelle Glangetas[1] ✉, Adriane Guillaumin[1], Elodie Ladevèze[1], Anaelle Braine[1], Manon Gauthier[1,2], Léa Bonamy[1], Evelyne Doudnikoff[1], Thibault Dhellemmes[1], Marc Landry[1], Erwan Bézard[1], Stephanie Caille[3], Anne Taupignon[1], Jérôme Baufreton[1] & François Georges[1] ✉

The Insula functions as a multisensory relay involved in socio-emotional processing with projections to sensory, cognitive, emotional, and motivational regions. Notably, the interhemispheric projection from the Insula to the contralateral Insula is a robust yet underexplored connection. Using viral-based tracing neuroanatomy, ex vivo and in vivo electrophysiology, in vivo fiber photometry along with targeted circuit manipulation, we elucidated the nature and role of Insula^{Ins} communication in social and anxiety processing in mice. In this study, we 1) characterized the anatomical and molecular profile of the Insula^{Ins} neurons, 2) demonstrated that stimulation of this neuronal subpopulation induces excitation in the Insula interhemispheric circuit, 3) revealed that Insula^{Ins} neurons are essential for social discrimination after 24 h of isolation in male mice. In conclusion, our findings highlight Insula^{Ins} neurons as a distinct class of neurons within the insula and offer new insights into the neuronal mechanisms underlying social behavior.

The Insular Cortex is classically described as an integrator of multimodal sensory signals coming from external cues (the environment) and internal cues (the body changes). For example, Insula responds to auditory or tactile cues[1] and cardiac interoceptive signals[2]. Interacting with novel individuals is an experience that leads to the integration of signals from both interoceptive and exteroceptive sources. Recently, it has been shown that some Insula cells respond to social interaction[3]. Interestingly these "social-on" cells solely represent a subset of Insula neurons that remained unexplored. In physiological situations, Insula neurons are engaged in social interaction and notably in social affective behaviors[4–9]. For example, it has been highlighted that Insula neurons projecting to the nucleus accumbens core regulate the social approach to stressed juvenile rats[8]. Autism spectrum Disorders (ASD) and Anxiety Disorders are pathologies with sensory integration defects that have been associated with dysfunction of the Insula[1,10–13]. An Insula maturation deficit was detected in a mouse model of ASD which is notably characterized by social interaction deficits, leading to an alteration in the integration of sensory information within the Insula[1]. Moreover, clinical studies show an Insula overactivation in anxious patients[10,14]. Altogether, these studies suggest that Insula is well-positioned to integrate and participate in regulating socio-emotional processing. Indeed, the Insula shares multiple projections with sensory and interoceptive regions (sensory cortex, thalamus, olfactory bulb), with cognitive regions (medial prefrontal cortex, orbitofrontal cortex), emotional territories (amygdala, bed nucleus of the stria terminalis), and motivation-associated structures (ventral tegmental area, nucleus accumbens)[15].

A strong but understudied projection is the Insula interhemispheric projection to the contralateral Insula[16], which will be referred to as Insula^{Ins} throughout the manuscript. As alteration in interhemispheric communication is associated with a social deficit[17–20], we

[1]Univ. Bordeaux, CNRS, IMN, Bordeaux, France. [2]Univ. Poitiers, Inserm, LNEC, Poitiers, France. [3]Univ. Bordeaux, CNRS, INCIA, Bordeaux, France.
✉e-mail: christelle.glangetas@u-bordeaux.fr; francois.georges@u-bordeaux.fr

postulated that Insula interhemispheric communication may be enrolled in social behavior processes.

Recent evidence points toward a crucial role of cortical interhemispheric communication in complex cognitive and emotional processing. For example, individuals with high anxiety levels present an altered interhemispheric communication in reaction to the presentation of emotional images[21]. Across mammalian evolution, cortical interhemispheric communication occurs notably through the corpus callosum[22]. Alterations in callosal fiber integrity have been observed in several pathological conditions as in patients with strokes, multiple sclerosis, schizophrenia, or ASD[23,24]. Despite recent advances in Insula participation in social behavior, the anatomical and molecular profile and the role of the Insula interhemispheric circuit in this socio-emotional processing remained poorly understood.

We hypothesized that Insula interhemispheric communication is essential to regulate social interactions and anxiety phenotype, and alteration in this communication would lead to social impairments and maladaptive anxiety behavior. To define the critical, yet unknown role of the Insula interhemispheric circuit, we used a combination of innovative neurotechniques, ex vivo and in vivo electrophysiology, in vivo fiber photometry and behavioral assays coupled with selective genetic neuron ablation and circuit manipulation in mice. This study was developed around 3 specific objectives: (i) Anatomical and molecular characterization of Insula^{Ins} neurons, (ii) Synaptic and circuit properties of Insula interhemispheric communication, (iii) Role of Insula interhemispheric communication in social interaction and anxiety-related behaviors in mice.

Results

Insula^{Ins} neurons represent a unique subpopulation of the Insula

We first confirmed that Insula project to multiple brain regions by using an anterograde monosynaptic viral approach (Supplementary Fig. 1a). Interestingly, we observed a strong bilateral innervation to the dorsolateral part of the bed nucleus of the stria terminalis (dlBNST), the Central Amygdala (CeA), and contralateral labeling to the Insula (Supplementary Fig. 1b–f). Next, we injected a retrograde monosynaptic virus into the Insula of AI9-dTomato mice (rAAV2-retro-CAG-cre virus; Fig. 1a). We detected tomato-positive neurons in the contralateral Insula, indicating the presence of Insula^{Ins} neurons that represent the homotopic connection (Fig. 1b and Supplementary Fig. 1g). We quantified that 85.92 ± 2.64% of cortical contralateral labeling was located in the homotopic cortical region and 14.08 ± 2.64% in heterotopic cortical regions (Fig. 1c, d and Supplementary Fig. 1h). More precisely, we noted 44% of homotopic labeling in the intermediate Insula, 43% in the posterior Insula, and 13% in the anterior Insula (Fig. 1e). Insula^{Ins} neurons were mainly located in layer II/III (Fig. 1f). We found 70.93% of Insula^{Ins} neurons in layer II/III and 29.07% in layer V/VI. Interestingly, the expression of the rAAV2-retro-CAG-cre virus was visible two weeks after the injection in Ai9-dTomato mice exhibiting a similar pattern of expression as observed after a 4-week delay. (Supplementary Fig. 1i).

To identify the projection targets of this Insula to-Insula circuit, we first mapped Insula^{Ins} neuron outputs, by injecting a retrograde monosynaptic virus (rAAV2-retro-CAG-Cre) in the contralateral Insula coupled with an anterograde monosynaptic virus (AAV1-phSyn1(S)-FLEX_tdTomato-T2A-SypEGFP-WPRE) injection in the ipsilateral Insula (Fig. 1g). We demonstrated that Insula^{Ins} neurons also projected significantly to the dlBNST (ovBNST and juxtaBNST) and the CeA (Fig. 1h, i and Supplementary Fig. 2a, b). In addition, we targeted the same Insula^{Ins} neuron downstream outputs by injecting the retrograde monosynaptic virus in the contralateral Insula (Supplementary Fig. 2c–h, o) or in the CeA (Supplementary Fig. 2i–n, p) with the anterograde monosynaptic virus in the ipsilateral Insula. We confirmed that CeA-projecting Insula neurons also innervate both the dlBNST and the contralateral Insula (Supplementary Fig. 2l–p).

We next used the expression of the transcription factors Ctip2 and Satb2 to characterize the molecular profile of Insula^{Ins} neurons. The transcription factors Ctip2 and Satb2 have been identified as a key regulator of cortical development and are involved in the determination of neuronal identity during brain development[25]. We demonstrated that Ctip2 and Satb2 are strongly expressed in all layers of the insular cortex in adult mice (Supplementary Fig. 3a, b). Insula^{Ins} neurons identified with tomato labeling specifically colocalized with Satb2 molecular marker without any colocalization with Ctip2 (Tomato$^+$/Satb2$^+$ colocalization: 96.13 ± 1.91%, Fig. 2a, b). We next investigated whether Insula^{Ins} subpopulation presented a unique molecular and electrophysiological signature. We injected a retrograde monosynaptic tracer, the cholera toxin b (CTb) in the contralateral Insula, in the tail of the striatum, or in the BLA (Supplementary Fig. 4a–d). We found that Insula^{Ins} neurons and Insula neurons projecting to the tail of the striatum (Insula$^{Tail\ Striatum}$) are mainly Satb2$^+$ and Ctip2$^-$, while those projecting to the BLA (Insula^{BLA} mainly express the Ctip2$^+$ molecular marker (Supplementary Fig. 4e–j). We next compared the passive and active membrane properties of Insula^{Ins} and Insula$^{Tail\ Striatum}$ pyramidal neurons using ex vivo electrophysiology (Supplementary Fig. 5a, b). No distinctions in the active or passive electrophysiological properties of these two neuronal subpopulations could be observed (Supplementary Fig. 5c–k). We next determined whether Insula^{Ins} neurons are exclusively pyramidal neurons or if they could be GABAergic projection neurons. No colocalization of Insula interhemispheric neurons with parvalbumin (PV) or glutamic acid decarboxylase (GAD67) staining was detected (Supplementary Fig. 3c–e), thereby confirming with their electrophysiological properties that these Insula^{Ins} neurons belong to the category of excitatory pyramidal neurons.

By using in vivo electrophysiology in anaesthetized mice, we functionally confirmed the reciprocal connectivity between both Insula (Fig. 2c–e). Indeed, we recorded typical antidromic responses characterized by a collision test and, or high-frequency stimulation tests evoked by the electrical stimulation of their terminals in the contralateral Insula (Fig. 2c, d). Interestingly, we observed a large variability in the latencies of antidromic responses (ranging from 3 to 30 ms; Fig. 2e). One parameter influencing the action potential velocity conduction is the degree of myelination. Intriguingly, the Insula is a unique and specific cortical region that poorly expresses the myelin basic protein (MBP), an oligodendrocyte protein essential for the myelin wrapping of axons in adult mice (Fig. 2f). By using the double viral approach to identify Insula^{Ins} neurons (with GFP labeling) coupled with electron microscopy preparation, we showed that all Insula^{Ins} neurons observed had unmyelinated axons passing through the corpus callosum or the anterior commissure (Fig. 2h, i; 0 GFP$^+$ myelinated axons out of $n = 59$ GFP$^+$ neurons, $N = 4$ mice).

Altogether, we identified a new neuronal subpopulation in the Insula, the Insula^{Ins} neurons, corresponding to the interhemispheric pyramidal subpopulation. This subpopulation expresses the molecular marker Satb2, exhibits bilateral projections to both dlBNST and CeA, is primarily situated in layer II/III, and has the peculiarity of having unmyelinated axons.

Insula^{Ins} neurons provide a synaptic-excitatory drive on the Insula interhemispheric circuit

We demonstrated that Insula^{Ins} neurons make asymmetric synapses, which are excitatory in function, with the contralateral Insula, the CeA, and the dlBNST (Fig. 3a–d). Insula to CeA and dlBNST synapses have been previously described[26–30]. However, the Insula to Insula synapses remained poorly characterized. Studies that have functionally studied interhemispheric synaptic transmission have mainly studied the motor cortex and have demonstrated the importance of inhibition of the contralateral cortex in the execution of lateralized movements[31–33]. The Insula is involved in integrating exteroceptive and interoceptive

https://doi.org/10.1038/s41467-024-51389-4

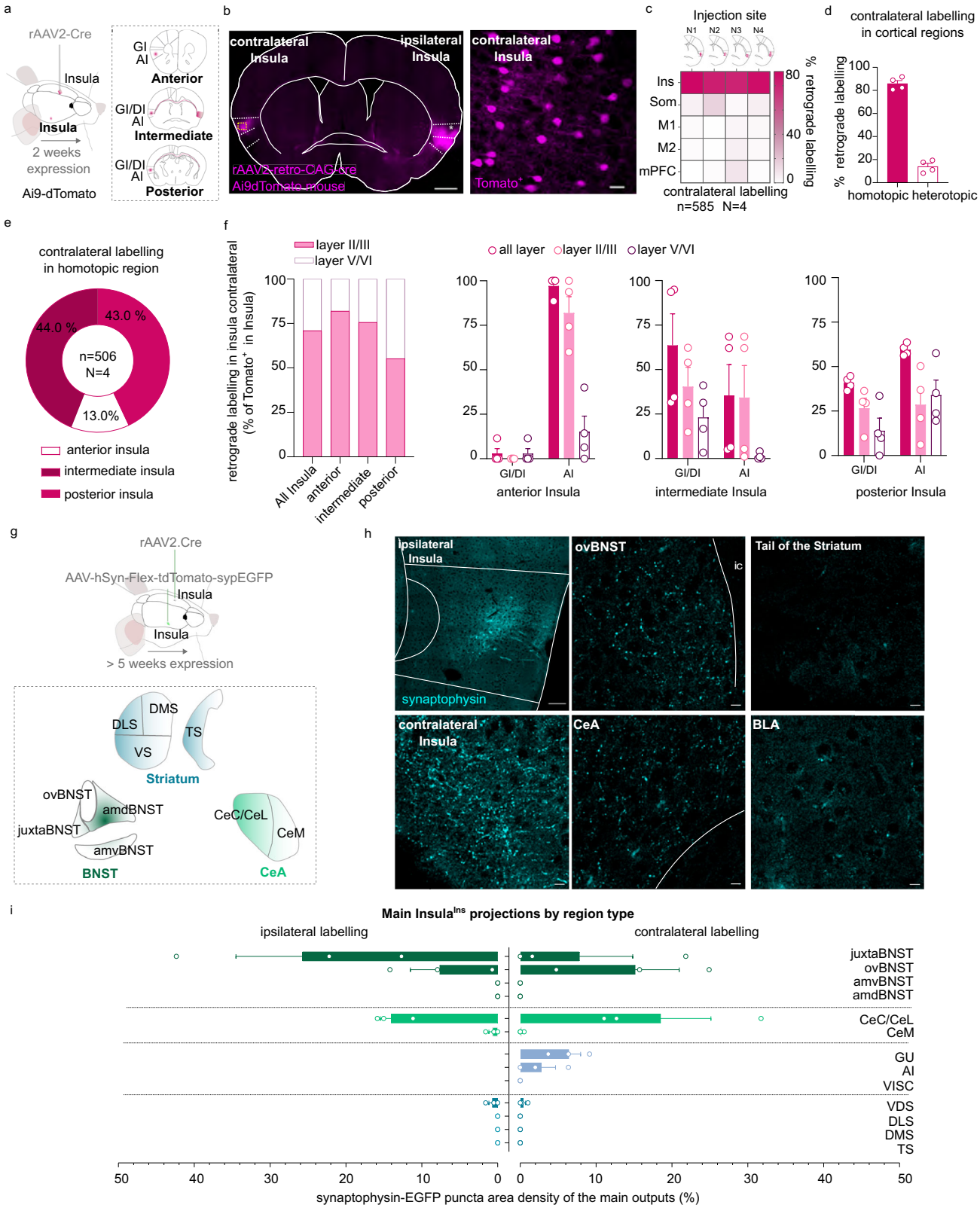

signals, contralateral inhibition does not seem necessary for the execution of emotional tasks. To complete our anatomical data, we tested the hypothesis that Insula stimulation may trigger an excitation in the contralateral Insula side by using ex vivo and in vivo electrophysiology in mice. First, we recorded contralateral Insula pyramidal neuron responses evoked by ipsilateral Insula optogenetic stimulation by using ex vivo electrophysiology (Fig. 3e–g). All the Insula neurons that we recorded were located in a dense zone of eYFP fibers and all of them respond to the Insula contralateral optogenetic stimulation. We found that 87.5% of the total recorded Insula pyramidal neurons respond by an excitation followed by inhibition to the ipsilateral Insula fiber optogenetic stimulation while 12.5% of these pyramidal neurons respond only by an excitation (Fig. 3h–j; EPSC amplitude -267.9 ± 41.64 pA; IPSC amplitude 582.1 ± 125.9 pA). In addition, only inhibitory

https://doi.org/10.1038/s41467-024-51389-4

Fig. 1 | Anatomical characterization of an Insula interhemispheric neuronal subpopulation. a, **g** Experimental design. **b** Representative epifluorescent image of a coronal slice of brain injected with a rAAV2-retro-CAG-Cre retrograde virus in the ipsilateral insula in Ai9-dTomato mouse (scale 500 μm) with a high magnification of contralateral labeling in Insula (example of the mouse N2, scale 25 μm). **c**, **d** Quantification of contralateral labeling in Insula (homotopic labeling) and other cortical regions (heterotopic labeling) in 4 mice (N1, N2, N3, N4). **e**, **f** Quantification of contralateral labeling in the homotopic Insula subregions (**e**), and layers (**f**) ($n = 506$ neurons, 4 mice). **h**, **i** immunofluorescence confocal images showing the Insula^{Ins} main projections identified by synaptophysin-eGFP puncta(h) and its quantification (**i**) ($N = 3$ mice). amdBNST anteromedialdorsal bed nucleus of the stria terminalis, amvBNST anteromedialventral bed nucleus of the stria terminalis, ovBNST oval-BNST, juxta-BNST juxtacapsular BNST, a.c. anterior commissure, cc corpus callosum, BLA basolateral amygdala, CeC/CeL central and lateral part of the central amygdala, CeM medial part of the central amygdala, DLS dorsolateral striatum, DMS dorsomedial striatum, VS ventral striatum, TS tail of the striatum, Ins Insula, Som Somatosensory cortex, M1 primary Motor cortex, M2 secondary Motor cortex, mPFC medial Prefrontal cortex, n number of neurons, *N* number of mice. Data are presented as mean values ± SEM.

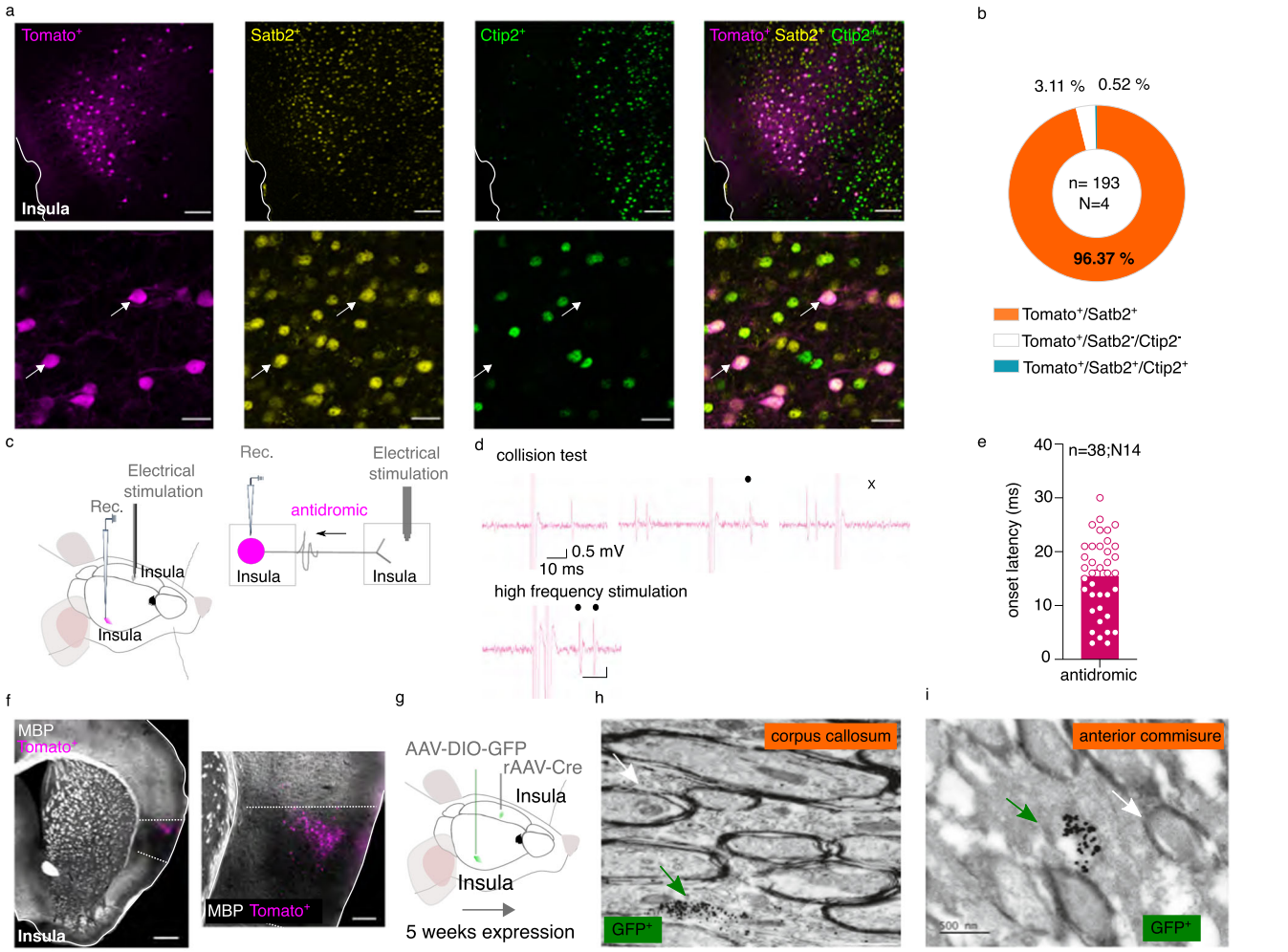

Fig. 2 | Molecular and electrophysiological characterization of Insula^{Ins} neurons. a Immunofluorescence confocal images showing Insula^{Ins} neurons (tomato labeling), insula Satb2 staining (yellow labeling), insula Ctip2 labeling (green labeling), and the overlay at low (top, scale 100 μm) and high magnification (bottom, scale 25 μm). At the bottom, white arrows show examples of Tomato and Satb2 colocalizations. **b** Quantification of Tomato, Satb2, and Ctip2 colocalization in the Insula. **c**, **g** Experimental design. **d** Representative traces showing a collision test and a high-frequency stimulation protocol for an Insula interhemispheric neuron projecting to the other Insula. **e** Histogram of the onset latency of Insula antidromic responses. **f** Representative epifluorescent image at low (left, scale bar 500 μm) and high magnification (right, 150 μm) of MBP staining (gray labeling) and Insula^{Ins} neurons (tomato labeling, $N = 3$ mice). **h**, **i** Representative image obtained with electron microscopy showing immunogold GFP labeling of unmyelinated Insula^{Ins} axons passing through the corpus callosum (**h**) or the anterior commissure (**i**) (green arrow, $N = 4$ mice). The white arrow shows an example of a myelinated axon (scale 500 nm). Rec recording, MBP myelin basic protein, *n* number of neurons, *N* number of mice. Data are presented as mean values ± SEM.

current is blocked by TTX and 4AP pharmacological cocktail bath application suggesting that excitatory transmission is monosynaptic while inhibitory current is polysynaptic (Fig. 3k; EPSC amplitude in aCSF: −242.8 ± 59.29 pA; EPSC amplitude in TTX + 4AP: −247.3 ± 101.8 pA; IPSC amplitude in aCSF: 508.2 ± 123.4 pA; IPSC amplitude in TTX + 4AP: 5.167 ± 5.02 pA). IPSC response latency is also delayed compared to EPSC response latency (EPSC latency: 1.88 ± 0.22 ms; IPSC latency: 4.46 ± 0.25 ms, Fig. 3l). These data suggest that activation of Insula^{Ins} neurons drives monosynaptic excitation on Insula contralateral pyramidal neurons followed by a polysynaptic feedforward inhibition.

Secondly, to decipher the net in vivo integrative effect of Insula interhemispheric transmission, we performed in vivo electrophysiology in anaesthetized mice (Fig. 3m). We observed that 32.73% of all contralateral Insula recorded neurons respond to ipsilateral Insula electrical stimulation (Fig. 3p). These Insula-responsive neurons are characterized by a half-action potential width of 1.08 ± 0.03 ms and a spontaneous firing frequency of 0.78 ± 0.13 Hz (Fig. 3n, o). Insula

https://doi.org/10.1038/s41467-024-51389-4

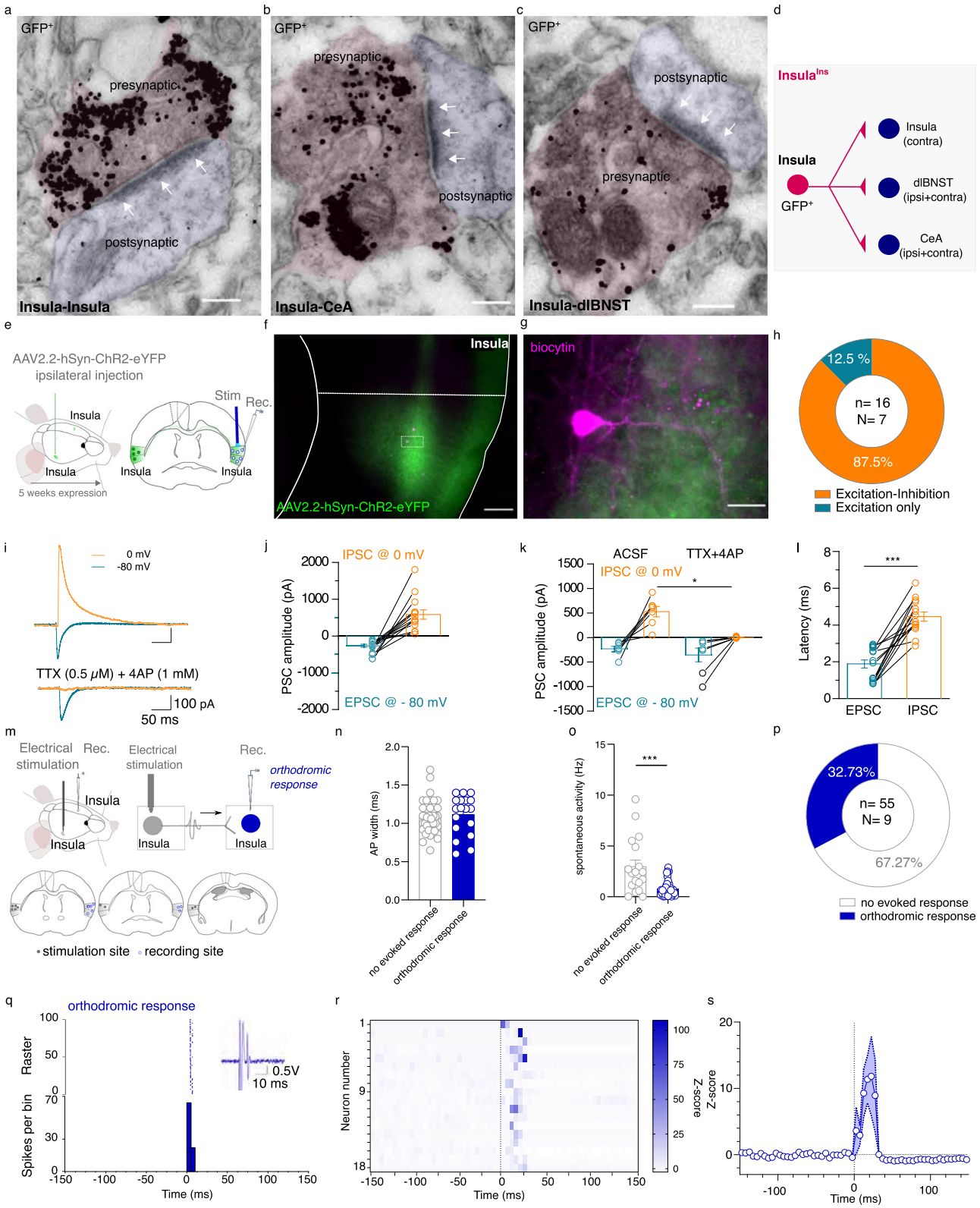

interhemispheric neuronal stimulation triggered excitatory responses on the contralateral Insula neurons with 10.61 ± 1.715 ms response latency (Fig. 3q–s). Remarkably, we didn't record in vivo Insula neurons that present both orthodromic and antidromic responses evoked by the contralateral Insula electrical stimulation.

Together, these results suggest that interhemispheric Insula neurons contact both excitatory and inhibitory contralateral Insula neurons, and feed-forward inhibition was activated within ~2.5 ms after the onset of excitation in both cell types, creating a precise temporal excitation in the Insula network.

Genetic selective ablation of Insula^{Ins} communication disrupts social preference following 24 h of social isolation

To determine whether Insula^{Ins} neurons play a role in social interaction, we measured mouse social interaction with a three-chamber social test in two different housing conditions associated with a caspase viral

Fig. 3 | Functional characterization of Insula^{Ins} circuit. a–c Representative images of immunogold GFP labeling obtained with electron microscopy showing asymmetric synapses (at white arrows) for Insula to Insula synapses (**a**), Insula to CeA synapses (**b**), and Insula to dlBNST synapses (scale bar: 150 nm, $N = 4$ mice). **d** Schematic representation of insula interhemispheric circuit. **e** Ex vivo electrophysiological experimental design. **f, g** Representative example of a histological control showing insula fibers expressing the Channelrhodopsin (green labeling) projecting to the contralateral insula and insula recorded neurons filled with biocytin (tomato labeling) at low (**f**, scale bar: 150 μm) and high magnification (scale bar: 25 μm). **h** Quantification of contralateral Insula pyramidal neuron responses to ipsilateral insula optogenetic stimulation. **i** Representative traces of evoked ESPC recorded at −80 mV and IPSC recorded at 0 mV in Insula pyramidal neuron before (top) and after TTX + 4AP bath application (bottom). **j, k** Group mean of evoked PSC amplitude of Insula pyramidal neurons (**j**) and after TTX + 4AP (**k**, IPSC amplitude aCSF vs TTX + 4AP: Wilcoxon test $W = 21$, $p = 0.0313$; EPSC amplitude aCSF vs TTX + 4AP: Wilcoxon test $W = 1$; $p > 0.05$). **l** Group mean of PSC response latency of Insula pyramidal neurons (Mann–Whitney test $U = 2$, $p < 0.0001$). **m** Experimental design (top) and cartography of stimulation and recording sites in the insula (bottom). **n, o.** Group mean of AP width (**n**) and spontaneous firing rate (**o**) of all the recorded insula neurons (Mann–Whitney test, $U = 147.5$, $p = 0.0006$). **p** Quantification of insula-responsive neurons to the electrical stimulation of the contralateral insula. **q** Typical PSTH and raster show a contralateral Insula-evoked excitatory response of an Insula neuron. Electrical stimulus at 0 ms, with 5 ms bin width. **r** Heatmap plot of Z-scored PSTH traces for each individual responsive Insula neuron to an Insula contralateral electrical stimulation. The electrical stimulus is represented by a vertical black line at 0 ms. **s** Mean Z-score of PSTH over all responsive insula cells. Stim stimulation, Rec recording, PSC postsynaptic current, EPSC excitatory PSC, IPSC inhibitory PSC, AP action potential. Data are presented as mean values ± SEM. $^{*}p < 0.05$, $^{***}p < 0.001$.

approach strategy to selectively lesion Insula^{Ins} neurons (Fig. 4a, b). Indeed, previous studies have shown that structures involved in the Insula interhemispheric network are recruited and display plastic adaptive neuronal responses after 24 h of isolation such as the dorsal raphe nucleus or the dlBNST[34,35]. To elucidate whether Insula^{Ins} neurons are crucial to develop adaptive social behavior after social isolation, we assessed social preference in group-housed conditions, 24 h and 2 weeks after social isolation in the control group mice and the caspase group. In two groups of mice, we injected a retrograde monosynaptic virus (rAAV2-retro-CAG-Cre) in two main outputs of the insula interhemispheric neurons (contralateral Insula and ipsilateral CeA) and an AAV-Flex-taCaspase-TEVp (caspase mice) or the control virus (AAV-Flex-eGFP; control mice) in the ipsilateral Insula (Fig. 4a). We first confirmed that the caspase viral strategy specifically lesioned Insula^{Ins} neurons as illustrated in the histological control example and quantified by NeuN fluorescence density in layer II/III of Insula (Fig. 4c–e). NeuN fluorescence density is specifically decreased in the layer II/III of the Insula caspase injection site compared to its contralateral Insula control site (Insula control site NeuN density: 44.15 ± 2.37; Insula caspase injection site NeuN density: 34.01 ± 2.86) without altering other proximal cortical regions as the somatosensory cortex (NeuN density in Somatosensory cortex control site: 31.28 ± 2.33; NeuN density in the other Somatosensory cortex site: 33.96 ± 0.91, Two-tailed paired t-Test $t(8) = 1.101$, $p > 0.05$). Under the group-housed condition, both control and caspase mice spent more time around the social enclosure compared to the object enclosure without differences in the three-chamber test (Fig. 4f, time spent around for ctrl: object 58.60 ± 6.84 s vs social 138.51 ± 9.86 s; caspase: object 58.83 ± 5.51 s vs social 133.43 ± 10.07 s; Two Way repeated measure Anova, zone × virus interaction effect $F(1,24) = 0.08521$, $p > 0.05$; zone main effect $F(1,24) = 72.09$, $p < 0.0001$; no virus main effect, F $(1,24) = 0.1018$, $p > 0.05$). Control and caspase male mice developed a social preference in the group-housed condition indicated by a social preference ratio >0.5 (Fig. 4g; ctrl social preference ratio: 0.70 ± 0.03 and caspase social preference ratio 0.69 ± 0.03; ctrl vs caspase social preference ratio, Mann–Whitney $U = 72$, $p > 0.05$). They spent a similar amount of time in the social zone (Fig. 4h, i; time in the social zone for ctrl: 46.17 ± 3.29%; for caspase: 44.48 ± 3.36%; two-tailed unpaired t-test, $t(24) = 0.3591$, $p > 0.05$; mean social bout duration for ctrl: 8.23 ± 0.84%; for caspase: 6.93 ± 0.86%; two-tailed unpaired t-test, $t(24) = 1.077$). Both groups displayed the same amount of time in grooming and rearing during the social interaction test (Fig. 4j, k; grooming: ctrl 2.52 ± 0.66% vs caspase 2.34 ± 0.41%, Mann–Whitney test, $U = 71$, $p > 0.05$; rearing: ctrl 4.05 ± 0.53% vs caspase 4.203 ± 0.63%, two-tailed unpaired t-test, $t(24) = 0.1831$, $p > 0.05$)

We next tested how social isolation affects attention to social stimuli in Insula^{Ins} lesioned male mice. After 24 h of social isolation, control mice spent more time around the social enclosure compared to the object enclosure while caspase mice spent the same time around both enclosures (Fig. 4l, time spent around for ctrl: object 76.53 ± 4.77 s vs social 126.35 ± 7.44 s; caspase: object 91.14 ± 7.17 s vs social 95.77 ± 8.04 s). Control group mice still presented social preference after 24 h of isolation contrary to caspase mice (Fig. 4m; ctrl social preference ratio: 0.62 ± 0.02 and caspase social preference ratio 0.51 ± 0.03). Caspase mice spent less time in the social zone compared to control mice only after 24 h of social isolation (Fig. 4n; time in the social zone for ctrl: 42.11 ± 2.48%; for caspase: 31.92 ± 2.68%). There was no difference in the mean social bout duration between groups (Fig. 4o; mean social bout duration for ctrl: 6.79 ± 0.78 s; for caspase: 5.34 ± 0.62 s; Two-tailed unpaired t-test, $t(24) = 1.420$ $p > 0.05$). No change was observed in the time spent in grooming and rearing during social interaction test (Fig. 4p, q; grooming: ctrl 1.52 ± 0.26% vs caspase 1.67 ± 0.40% two-tailed unpaired t-test, $t(24) = 0.3293$, $p > 0.05$; rearing: ctrl 6.35 ± 0.94% vs caspase 6.24 ± 1.30%, Mann–Whitney test, $U = 67$, $p > 0.05$). However, 5 min before the behavioral testing (during the isolation period), we noted an increase in grooming time in caspase mice compared to control mice only after 24 h of social isolation without changes in rearing and distance travelled (Supplementary Fig. 6a–f, in group-housed condition, grooming duration: ctrl 2.52 ± 0.65% vs caspase 1.93 ± 0.43%; Mann–Whitney test, $U = 78$, $p > 0.05$; rearing duration: ctrl 9.74 ± 1.94% vs caspase 8.31 ± 1.91%, Mann–Whitney test, $U = 68$, $p > 0.05$; distance travelled: ctrl 2423 ± 186.1 cm vs caspase 2328 ± 138.8 cm, two-tailed unpaired t-test $t(24) = 0.3997$, $p > 0.05$; in 24 h isolated condition: grooming duration: ctrl 0.66 ± 0.28% vs caspase 1.85 ± 0.51%; rearing duration: ctrl 15.27 ± 2.82% vs caspase 13.47 ± 2.12%, Mann–Whitney test, $U = 71$, $p > 0.05$; distance travelled: ctrl 2646 ± 184.4 cm vs caspase 2580 ± 208.1 cm, two-tailed unpaired t-test $t(24) = 0.2394$, $p > 0.05$). Interestingly, we found no behavioral differences between control and caspase female mice in the social interaction test, both in group-housed conditions and after 24 h of social isolation. (Supplementary Fig. 6g–r, group-housed condition: Supplementary Fig. 6g, time spent around for ctrl: object 60.53 ± 6.9 s vs social 97.11 ± 11.61 s; caspase: object 66.12 ± 3.85 s vs social 87.58 ± 5.04; Two Way repeated measure Anova, No zone x virus interaction effect $F(1,20) = 0.8371$, $p > 0.05$; zone main effect $F(1,20) = 12.34$, $p = 0.002$; no virus main effect, F $(1,20) = 0.05715$, $p > 0.05$; Supplementary Fig. 6h, ctrl social preference ratio: 0.61 ± 0.04 and caspase social preference ratio 0.57 ± 0.02; ctrl vs caspase social preference ratio, Two-tailed unpaired-test, $t(10) = 0.8803$, $p > 0.05$; One sample Wilcoxon test for ctrl: $W = 17$, $p > 0.05$, and caspase: $W = 19$, $p = >0.05$; Supplementary Fig. 6i; time in the social zone for ctrl: 32.37 ± 3.87%; for caspase: 29.19 ± 1.68%; two-tailed unpaired t-test, $t(10) = 0.753$, $p > 0.05$; Supplementary Fig. 6j–l; grooming: ctrl 0.98 ± 0.52% vs caspase 0.69 ± 0.35%, Mann–Whitney test, $U = 17$, $p > 0.05$; rearing: ctrl 3.69 ± 1.04% vs caspase 2.44 ± 0.55%, Mann–Whitney test, $U = 12$, $p > 0.05$; travelled distance: ctrl 2321 ± 178.3 cm vs caspase 2514 ± 141 cm, two-tailed unpaired t-test, $t(10) = 0.8482$, $p > 0.05$); in 24 h isolated condition: Supplementary

https://doi.org/10.1038/s41467-024-51389-4

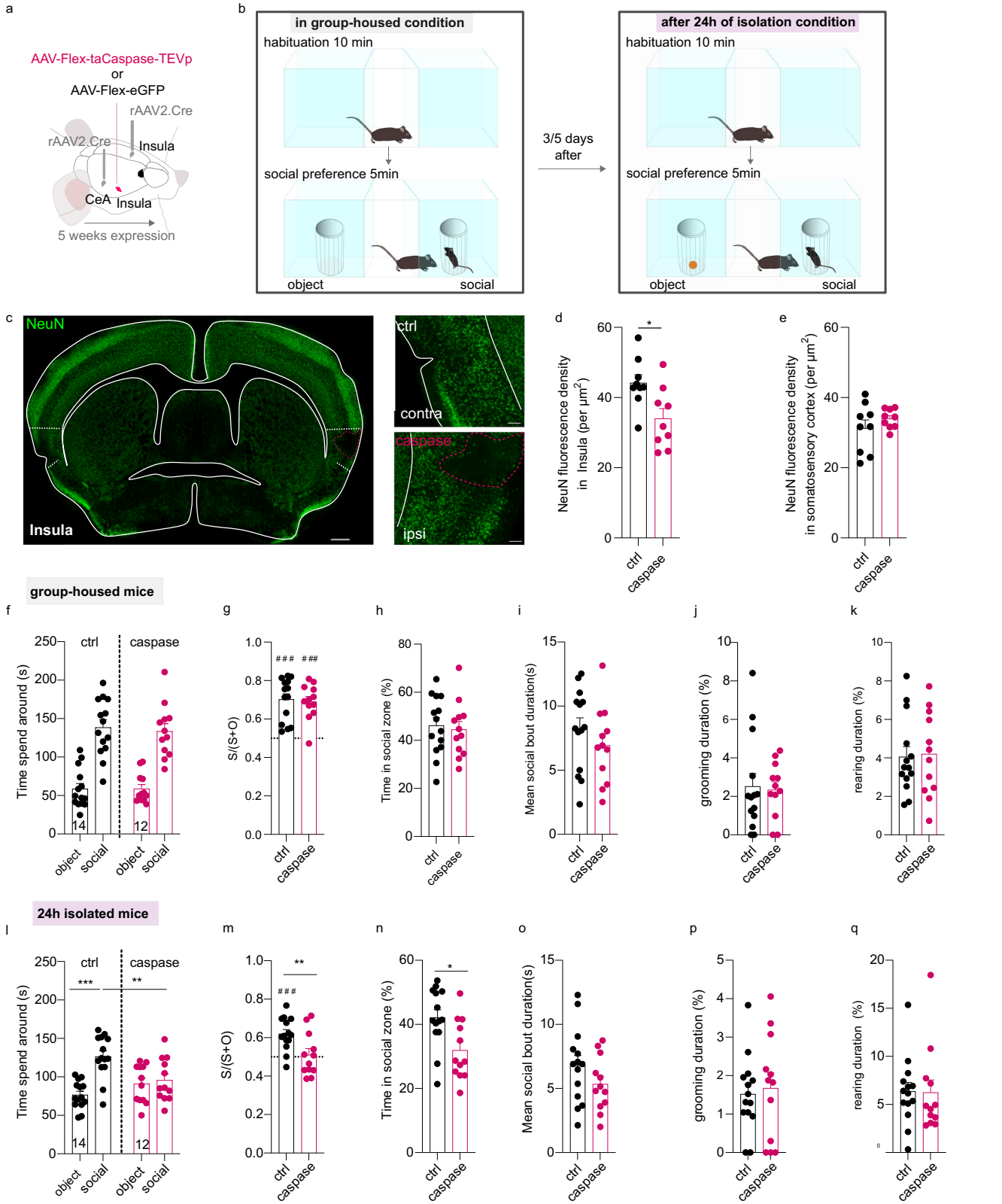

Fig. 6m, time spent around for ctrl: object 61.42 ± 10.32 s vs social 78.922 ± 12.37 s; caspase: object 47.14 ± 7.74 vs social 86.61 ± 5.99; Two Way repeated measure Anova, no zone x virus interaction effect $F(1,10) = 0.9601$, $p > 0.05$; zone main effect $F(1,10) = 6.461$, $p = 0.02$; no virus main effect, $F(1,10) = 0.2079$, $p > 0.05$; Supplementary Fig. 6n, ctrl social preference ratio: 0.56 ± 0.06 and caspase social preference ratio 0.65 ± 0.05; ctrl vs caspase social preference ratio, Two-tailed unpaired-test, $t(10) = 1.250$, $p > 0.05$; One sample Wilcoxon test for ctrl: $W = 11$, $p > 0.05$, and caspase: $W = 21$, $p < 0.05$; Supplementary Fig. 6o; time in the social zone for ctrl: 26.31 ± 4.12%; for caspase: 28.87 ± 2%; Mann–Whitney test, $U = 12$, $p > 0.05$; Supplementary Fig. 6p–r; grooming: ctrl 0.91 ± 0.38% vs caspase 0.91 ± 0.42%, two-tailed unpaired t-test $t(10) = 0.006513$, $p > 0.05$; rearing: ctrl 6.68 ± 1.4% vs caspase 7.02 ± 0.37%, two-tailed unpaired t-test, $t(10) = 0.2307$,

Fig. 4 | Selective genetic ablation of Insula^{Ins} neurons disrupts social preference only after 24 h of social isolation. a, **b** Experimental design for the viral injection (**a**) and behavioral assay (**b**). **c** Example of a histological control of caspase lesion in the insula identified by NeuN immunofluorescence labeling (green labeling) taken at epifluorescence microscope at low (left, scale bar: 500 μm) and high magnification (right, scale bar: 100 μm). **d**, **e** Quantification of NeuN fluorescence density in the control side (contralateral side to the injected lesion side, $N = 9$ mice) compared to the caspase injection side ($N = 9$ mice) in the Insula cortex (**d**, two-tailed Paired-*t*-test, $t(8) = 2.788$, $p = 0.0236$) and in the Somatosensory cortex (**e**). **f**, **l** Quantification of the time spent around the object and social enclosures in the three-chamber test in group-housed condition (**f**) or after 24 h of social isolation (**l**, two-way repeated measure Anova, Zone x virus interaction effect, $F(1,24) = 8.911$, $p = 0.0064$; zone main effect $F(1,24) = 12.94$, $p = 0.0014$; no virus main effect $F(1,24) = 1.685$, $p > 0.05$; Bonferroni *post hoc* test ctrl social vs caspase social $p = 0.0059$; ctrl social vs control object: $p = 0.0001$) in Insula control and Insula caspase groups. **g**, **m** Social preference ratio in the control group and caspase group in group-housed mice (**g**, one sample Wilcoxon test for ctrl: $W = 105$, $p = 0.0001$, and caspase: $W = 76$, $p = 0.001$) or isolated mice (**m**, two-tailed unpaired *t*-test, $t(24) = 2.806$, $p = 0.0098$; one sample *t*-test for ctrl: $t(13) = 5.211$, $p = 0.0002$; for caspase: $t(11) = 0.7564$, $p > 0.05$). **h**, **n** Time spent in the social zone between control and caspase mice in group-housed (h) or 24 hours-isolated conditions (**n**, two-tailed Unpaired *t*-test, $t(24) = 2.792$, $p = 0.0101$), **i**, **o** Mean social bout duration in control and caspase group in group-housed (**i**) and 24 hours-isolated housing condition (**o**). **j**, **k**, **p**, **q** Time spent in grooming and rearing in group-housed (**j**, **k**) or after 24 h of social isolation (**p**, **q**). ctrl control, S time in the social zone, O time in the object zone, contra contralateral, ipsi ipsilateral. Data are presented as mean values ± SEM. ### is used to mention a difference with a social preference ratio equal to 0.5. $^{*}p < 0.05$, $^{**}p < 0.01$,$^{***}p < 0.001$.

$p > 0.05$; travelled distance: ctrl 2848 ± 255.7 cm vs caspase 2678 ± 318.4 cm, two-tailed unpaired *t*-test, $t(10) = 0.4169$, $p > 0.05$). In addition, we observed no difference in social interaction between control and caspase male and female mice after chronic social isolation (Supplementary Fig. 7a–c, time spent around for ctrl: object 45.02 ± 3.73 s vs social 72.12 ± 7.95 s; caspase: object 51.92 ± 5.37 s vs social 67.6 ± 5.13 s; Two Way repeated measure Anova, no zone x virus interaction effect $F(1,16) = 0.7738$, $p > 0.05$; zone main effect $F(1,16) = 10.84$, $p = 0.0046$; no virus main effect, F $(1,16) = 0.05875$, $p > 0.05$; Supplementary Fig. 7b, ctrl social preference ratio: 0.61 ± 0.03 and caspase social preference ratio 0.57 ± 0.04; ctrl vs caspase social preference ratio, Two-tailed unpaired-test, $t(16) = 0.8416$, $p > 0.05$; Supplementary Fig. 7c; time in the social zone for ctrl: 24.04 ± 2.65%; for caspase: 22.53 ± 1.71%; Mann–Whitney test $U = 37$, $p > 0.05$).

Moreover, we also used an inhibitory chemogenetic viral approach to manipulate Insula^{Ins} neurons during social behavior in group-housed mice, or in 24-hour or 2-week isolated male and female mice (Fig. 5a, b). We performed an intraperitoneal injection of CNO (1 mg/kg) 30 min before the social behavior test. There were no differences in social behavior when we decreased the excitability of Insula^{Ins} mice during the three-chamber social test in group-housed neither in 24 h nor 2-week social isolation conditions (Fig. 5c–g; group-housed condition, Fig. 5c, time spent around for ctrl: object 48.38 ± 5.21 s vs social 82.94 ± 5.24 s; caspase: object 46.78 ± 2.17 s vs social 90.21 ± 6.66 s; Two Way repeated measure Anova, no zone x virus interaction effect $F(1,36) = 0.6834$, $p > 0.05$; zone main effect $F(1,36) = 52.81$, $p < 0.0001$; no virus main effect, F $(1,36) = 0.2794$, $p > 0.05$; Fig. 5d; ctrl social preference ratio 0.63 ± 0.03 and caspase social preference ratio 0.65 ± 0.02; ctrl vs caspase social preference ratio, two-tailed unpaired *t*-test, $t(18) = 0.4427$, $p > 0.05$; 24 h isolated condition, Fig. 5e, time spent around for ctrl: object 37.65 ± 1.68 s vs social 70.59 ± 5.28 s; hM4Di: object 44.26 ± 2.66 s vs social 74.45 ± 9.04 s; Two Way repeated measure Anova, no zone x virus interaction effect $F(1,36) = 0.07223$, $p > 0.05$; zone main effect $F(1,36) = 38.14$, $p < 0.0001$; no virus main effect, F $(1,36) = 1.048$, $p > 0.05$; Fig. 5f; ctrl social preference ratio 0.64 ± 0.02 and caspase social preference ratio 0.61 ± 0.04; ctrl vs caspase social preference ratio, two-tailed unpaired *t*-test, $t(18) = 0.7952$, $p > 0.05$; 2 weeks isolated condition, Fig. 5g, time spent around for ctrl: object 55.76 ± 8.21 s vs social 48.60 ± 7.76 s; hM4Di: object, 53.15 ± 6.93 s vs social, 61.82 ± 9.37 s; Two Way repeated measure Anova, no zone × virus interaction effect $F(1,36) = 0.8839$, $p > 0.05$; no zone main effect $F(1,36) = 0.008029$, $p > 0.050$; no virus main effect, F $(1,36) = 0.3968$, $p > 0.05$; Fig. 5h, ctrl social preference ratio 0.47 ± 0.06 and hM4Di social preference ratio 0.53 ± 0.06; ctrl vs caspase social preference ratio, Mann–Whitney $U = 35$, $p > 0.05$).

Insula is activated during anxious situations and Insula overactivation has been detected in patients with Anxiety disorders[11,14,36–40]. Since Insula interhemispheric neurons project to CeA and dlBNST, we next investigated the impact of Insula^{Ins} lesion on unconditioned anxiety tests in mice. In rodents, anxiety can be measured based on the innate approach/avoidance behavior in a novel environment. We didn't detect a change in the time spent and the number of visits in the center of the open field, nor in the total distance travelled (Supplementary Fig. 8a, b, Time spent in the center for ctrl: 16.65 ± 2.06%; caspase: 17.47 ± 1.45%, two-tailed unpaired *t*-test, $t(18) = 0.3088$, $p > 0.05$; the number of visits in the center for ctrl: 57.45 ± 5.42 visits; caspase: 62.89 ± 4.26 visits, two-tailed unpaired *t*-test, $t(18) = 0.7612$, $p > 0.05$; total distance travelled for ctrl: 4367 ± 309.3 cm; caspase: 4526 ± 214.2 cm, two-tailed unpaired *t*-test, $t(18) = 0.404$, $p > 0.05$). In addition, we didn't observe a difference in the time spent and the number of entries in the open arms in the elevated plus maze nor in the total distance travelled between control and caspase mice (Supplementary Fig. 8c, d, Time spent in the open arms, ctrl: 4.47 ± 1.01%; caspase: 5.24 ± 1.37%, Mann–Whitney, $u = 41.5$, $p > 0.05$; the number of entries in the OA for ctrl: 4.091 ± 0.72 visits; caspase: 3.89 ± 0.89 visits, Two-tailed Unpaired-*t*-test, $t(18) = 0.1788$, $p > 0.05$; total distance travelled for ctrl: 967 ± 80.99 cm; caspase: 1117 ± 69.14 cm, Two-tailed unpaired *t*-test, $t(18) = 1.375$, $p > 0.05$). In parallel, we also manipulated Insula^{Ins} neurons with excitatory and inhibitory chemogenetic viral approaches to evaluate the effect on anxiety (Supplementary Fig. 8e, Fig. 5a). We validate chemogenetic viral approach by using ex vivo electrophysiology (Supplementary Fig. 8g). We confirmed that CNO bath application increased the excitability of Ins^{Ins} cells expressing the AAV-DIO-hM3D-mCherry virus. After the CNO bath application, Ins^{Ins} neurons were more depolarized and presented an increase in their spontaneous firing rate. No alterations were observed in the open field test (Supplementary Fig. 8h, i, total distance: ctrl 4646 ± 377.4 cm vs hM3D 4557 ± 231.7 cm, two-tailed unpaired *t*-test, $t(14) = 0.1874$, time spend in the center: ctrl: 4.50 ± 0.76% vs hm3D 5.15 ± 0.95%, Mann–Whitney, $U = 23$, $p > 0.05$, number of entries in the center: ctrl 34.33 ± 4.85 entries vs hM3D 37.86 ± 5.05 entries, Mann–Whitney, $U = 22.50$, $p > 0.05$; Fig. 5i, j, total distance: ctrl 4391 ± 236.6 cm vs hM4Di 4468 ± 225.7 cm, two-tailed unpaired *t*-test, $t(18) = 0.2251$, $p > 0.05$, time spend in the center: ctrl 6.83 ± 0.95% vs hM4Di 8.44 ± 1.96%, two-tailed unpaired *t*-test, $t(18) = 0.8213$, $p > 0.05$. There were no differences in the elevated plus maze between groups (Supplementary Fig. 8j, k; time in open arms: ctrl 8.8 ± 1.42% vs hM3D 7.36 ± 1.71%, two-tailed unpaired *t*-test, $t(14) = 0.6516$, $p > 0.05$, number of entries in open arms: ctrl 10.78 ± 1.79 entries vs hM3D 11.57 ± 2.06 entries, two-tailed unpaired *t*-test, $t(14) = 0.2913$, $p > 0.05$; Fig. 5k, l, time in open arms: ctrl 11.18 ± 1.77% vs hM4Di 15.27 ± 1.37%, two-tailed unpaired *t*-test, $t(18) = 1.671$, $p > 0.05$, number of entries in open arms: ctrl 10.25 ± 0.94 entries vs hM4Di 11.25 ± 1.51 entries, two-tailed unpaired *t*-test, $t(18) = 0.5954$, $p > 0.05$). However, there was an increase in the time spent in the light compartment in the light–dark box test in hM3D Insula^{Ins} mice compared to their control groups

https://doi.org/10.1038/s41467-024-51389-4

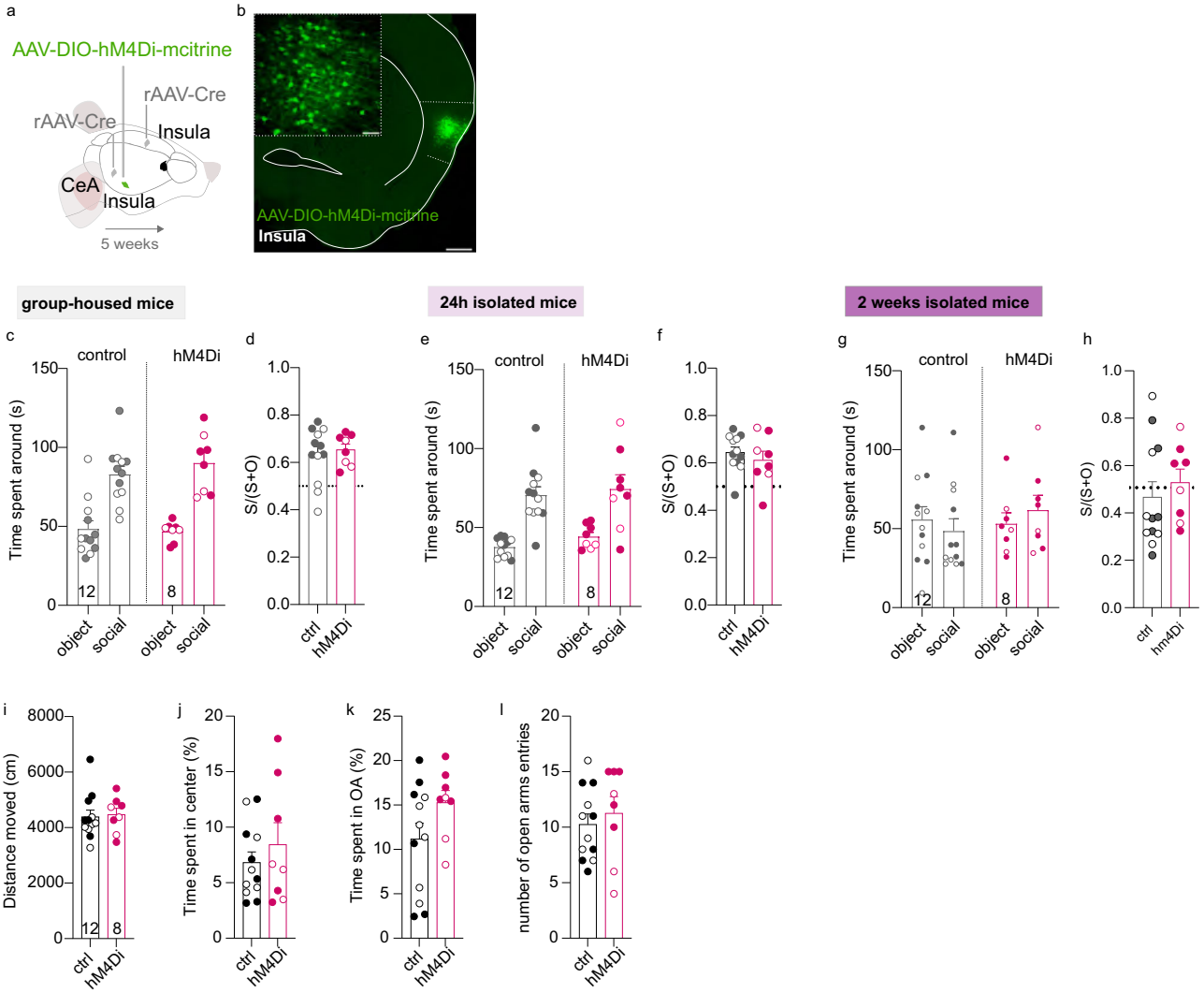

Fig. 5 | Chemogenetic inhibition of Insula^{Ins} neurons during the three-chamber social interaction test does not block social preference. a Experimental design. **b** Histological control showing an example of AAV8-hSyn-DIO-HA-hM4D(Gi)-IRES-mCitrine injection site in the Insula coupled with rAAV2-CAG-cre injection in the Insula contralateral and the CeA (low magnification, scale: 500 μm, high magnification, scale: 50 μm). **c**, **e**, **g** Quantification of the time spent around the object and social enclosures in the three-chamber test in Insula control and Insula hM4Di male and female mice in group-housed (**b**), 24 h isolated (**e**), and 2 weeks isolated mice (**g**). **d**, **f**, **h** Social preference ratio in the control group and caspase group in group-housed mice (**d**) or 24 h isolated (**f**) or 2 weeks isolated mice (**h**). **i**, **j** Quantification of the total distance travelled (**i**) and the time spent in the center of the open field (**j**) in control and hM4Di male and female mice. **k**, **l** Quantification of the time spent (**k**) and the number of entries (**l**) in the open arms of the elevated plus maze in both groups. (white circle: female, dark circle: male). Numbers in the histogram bars indicate the number of mice. Data are presented as mean values ± SEM.

without changes in the latency to the first visit in the light (Supplementary Fig. 8m, time in the light compartment: ctrl 52.12 ± 3.5% vs hM3D 66.54 ± 2.51%; number of entries in the light compartment: ctrl 19.56 ± 1.48 entries vs hM3D 22.71 ± 2.87 entries, two-tailed unpaired *t*-test, $t(14) = 1.045$, $p > 0.05$, latency to first visit in light: ctrl 7.56 ± 2.41 s vs hM3D 5.24 ± 1.7 s, two-tailed unpaired *t*-test, $t(13) = 0.7661$, $p > 0.05$). Moreover, there was a similar performance in the marble burying test and novelty-suppressed feeding behavior between control and hM3D Insula^{Ins} mice (Supplementary Fig. 8n, o, marble buried: ctrl 3.56 ± 0.96 marbles buried vs hM3D 3.43 ± 0.81 marbles buried, two-tailed unpaired *t*-test, $t(14) = 0.09728$, $p > 0.05$; Supplementary Fig. 8p latency to eat food: ctrl 72 ± 6.27 s vs hM3D 82.71 ± 15.66 s, two-tailed unpaired *t*-test, $t(14) = 0.6942$, $p > 0.05$).

Furthermore, we showed that lesion of Insula^{Ins} neurons does not alter motivation for a natural reward (Supplementary Fig. 9). Mice were trained on FR1, FR2, and FR5 for sweet condensed milk (scm) (Supplementary Fig. 9a–c). Results indicated that control and caspase mice have acquired similar levels of active responding over the different schedules of reinforcement (Supplementary Fig. 9a, two-way ANOVA, global interaction $F(2,30) = 0.30$, $p > 0.05$; group effect $F(1,30) = 0.003$, $p > 0.05$). Moreover, for both groups, the total number of active nose-pokes significantly increased over the FRs (Fixed ratio effect, $F(2,30) = 8.39$, $p < 0.001$). Visits in the inactive operandum were low across groups and across sessions (Supplementary Fig. 9b, two-way ANOVA, global interaction $F(2,30) = 0.54$, $p > 0.05$; group effect $F(1,30) = 0.04$, $p > 0.05$ and fixed ratio effect $F(2,30) = 1.67$, $p > 0.05$). Finally, the total number of rewards obtained by control and caspase mice followed the same trends as the visits in the active nose-poke (Supplementary Fig. 9c, two-way ANOVA, global interaction $F(2,30) = 1.12$, $p > 0.05$; group effect $F(1,30) = 0.030$, $p > 0.05$ and fixed ratio effect $F(2,30) = 3.50$, $p < 0.04$). Lesion-induced differences in motivation for scm were tested using a progressive ratio schedule of reinforcement; results are presented in Supplementary Fig. 9d, e. ANOVA analysis on the total number of active nose-pokes indicated that caspase lesion did not change the response rate during the PR session (Supplementary Fig. 9d; global interaction $F(1,10) = 1.39$,

$p > 0.05$; group effect F (1,10) = 3.61, $p > 0.05$, session effect F (1,10) = 3.61, $p > 0.05$). In addition, the caspase lesion did not alter the breaking point for scm compared to control mice (Supplementary Fig. 9e; global interaction (F (1,10) = 0.08, $p > 0.05$; group effect F (1,10) = 3.27, $p > 0.05$). Notably, both groups showed higher performances in the second PR session (Supplementary Fig. 9e, session effect F (1,10) = 23.88, $p = 0.001$).

Collectively, these data show that Insula^{Ins} neuronal alteration leads to impairment of social preference only after 24 h of social isolation in male mice without interfering with anxiety-like behaviors.

Because we didn't inhibit social preference while reducing the excitability of Insula^{Ins} neurons during the social interaction test, we hypothesized that the changes in Insula^{Ins} neuron activity likely occurred during the 24-hour period of social isolation instead. To test this, we first recorded the ex vivo activity of Insula^{Ins} neurons identified by a tomato labeling (retrograde monosynaptic virus rAAV2-retro-CAG-tdTomato injected in the contralateral Insula, Fig. 6a, b) in group-housed and 24-hour isolated mice. Interestingly, we found a decrease in the rheobase of Insula^{Ins} neurons of isolated mice compared to group-housed (rheobase, group-housed: 80.43 ± 12.83 pA vs isolated: 55 ± 7.73 pA, Fig. 6a, c). The resting membrane potential of Insula^{Ins} neurons is increased after 24 h of social isolation (Vm, group-housed: −71.13 ± 1.04 mV vs isolated:-67.88 ± 0.74 mV, Fig. 6d). Insula^{Ins} neuron resistance is increased in isolated conditions compared to group-housed conditions (Rm, group-housed: 285.4 ± 21.14 MΩ vs isolated: 383.8 ± 35.18 MΩ, Fig. 6e).

Based on our previously mentioned results, we finally wondered whether Insula^{Ins} neurons encode social behavior. To address this, we recorded the in vivo calcium activity using fiber photometry of Insula^{Ins} neurons during social interactions in both group-housed and isolated conditions (Fig. 6f–h and Supplementary Figs. 10 and 11). We injected a rAAV2-retro-CAG-Cre retrograde virus in the contralateral Insula with an AAV9-syn-Flex-jGCAMP8f-WPRE or an AAV9-pCAG-Flex-eGFP-WPRE in the ipsilateral Insula (Fig. 6f, g). We confirmed that mice develop a social preference in both group-housed and 24-hour social isolation in the three-chamber social interaction test (Fig. 6 i, group-housed: time spent around social:129.2 ± 6.59 s vs object 72.92 ± 6.95 s, Fig. 6j, 24 h isolated social 121 ± 10.35 s vs object 59.80 ± 4.65 s). We observed a difference in the Z-score of dF/F in calcium signaling in Insula^{Ins} neurons when the mouse was around a social enclosure compared to the object enclosure only 24 h after social isolation (Fig. 6k–q, group-housed: z-score dF/F of Insula^{Ins} Ca^{2+} neurons around social: 0.023 ± 0.01 vs object 0.028 ± 0.02; 24 h isolation z-score dF/F of Insula^{Ins} Ca^{2+} neurons around social: 0.036 ± 0.01 vs object −0.043 ± 0.02). In particular, we detected these differences, especially during the last sessions of interactions in the three-chamber test (Supplementary Fig. 10 a, group-housed: z-score dF/F of Insula^{Ins} Ca^{2+} neurons around social: 0.046 ± 0.045 vs object 0.013 ± 0.06 x; 24 h isolation z-score dF/F of Insula^{Ins} Ca^{2+} neurons around social: 0.06 ± 0.04 vs object -0.013 ± 0.018; Two Way repeated measure Anova, Interaction $F(1,6) = 0.1887$, $p > 0.05$, no main effect of housing $F(1,6) = 0.02373$, $p = 0.8826$, no main effect of zone $F(1,6) = 1.484$, $p > 0.05$; Supplementary Fig. 10b, group-housed: z-score dF/F of Insula^{Ins} Ca^{2+} neurons around social: 0.043 ± 0.047 vs object 0.095 ± 0.07; 24 h isolation z-score dF/F of Insula^{Ins} Ca^{2+} neurons around social: 0.12 ± 0.04 vs object -0.03 ± 0.028). Specifically, we observed no difference in the Ca^{2+} levels of Insula^{Ins} neurons between the habituation phase and the social interaction phase of the social three-chamber test in both group-housed mice and 2-weeks isolated mice. (Supplementary Fig. 11a, Group-housed habituation time: z-score dF/F of Insula^{Ins} Ca^{2+} neurons around social 0.003 ± 0.041 vs object -0.004 ± 0.042; group-housed social interaction time z-score dF/F of Insula^{Ins} Ca^{2+} neurons around social 0.023 ± 0.01 vs object 0.028 ± 0.02; Two Way repeated measure Anova, no Interaction $F(1,6) = 0.06076$, $p > 0.05$, no main effect of time $F(1,6) = 0.3051$, $p > 0.05$, no main effect of zone $F(1,6) = 0.003144$, $p > 0.05$; Supplementary Fig. 11k,2 weeks isolation habituation time: z-score dF/F of Insula^{Ins} Ca^{2+} neurons around social 0.03 ± 0.041 vs object −0.012 ± 0.027; 2 weeks social isolation social interaction time z-score dF/F of Insula^{Ins} Ca^{2+} neurons around social 0.019 ± 0.022 vs object −0.037 ± 0.11, Two Way repeated measure Anova, no Interaction $F(1,6) = 0.03583$, $p > 0.05$, no main effect of time $F(1,6) = 1.292$, $p > 0.05$, no main effect of zone $F(1,6) = 3.179$, $p > 0.05$). Only, 24 h after social isolation, we could observe an increase in the Z-score of df/F of Insula^{Ins} Ca^{2+} neurons when the mouse is around the social enclosure in the social interaction phase compared to the same location in the habituation phase (Supplementary Fig. 11f, 24 h isolated habituation time: z-score dF/F of Insula^{Ins} Ca^{2+} neurons around social −0.017 ± 0.02 vs object −0.018 ± 0.042; 24 h isolated social interaction time z-score dF/F of Insula^{Ins} Ca^{2+} neurons around social 0.036 ± 0.011 vs object-0.043 ± 0.021). There was a decrease in the peak of AUC in Insula^{Ins} Ca^{2+} neurons between social and object enclosure together with a decrease in the width of Ca^{2+} transient between social and object enclosure only in 24 hours-isolation condition (Supplementary Fig. 11b, group-housed condition peak AUC social 1.11 ± 0.17 vs object 1.083 ± 0.13, Wilcoxon test, $p > 0.05$, Supplementary Fig. 11g, 24 h isolation, peak AUC social 0.99 ± 0.13 vs object 0.66 ± 0.1; Supplementary Fig. 11l, chronic social isolation, peak AUC social 1.047 ± 0.15 vs object 0.91 ± 0.15, paired t-test, $t(5) = 1.420$, $p > 0.05$; Supplementary Fig. 11 d, group-housed condition width of Ca^{2+} transient, social 17.41 ± 2.15 vs object 17 ± 1.63, paired t-test, $t(6) = 0.1704$, $p > 0.05$, Supplementary Fig. 11i, 24 h isolation, width Ca^{2+} transient, social 15.87 ± 2.08 vs object 11.78 ± 1.68; Supplementary Fig. 11n, chronic social isolation, width Ca^{2+} transient, social 17.34 ± 2.27 vs object 15.39 ± 2.06, Wilcoxon test, $p > 0.05$).

Overall, we showed that Insula^{Ins} neurons are more excitable after 24-h of social isolation. Insula^{Ins} neurons presented a shift in calcium activity during the comparative exploration of a social and object stimulus in the three-chamber social interaction test only after 24-h of social isolation in mice.

Discussion

We unravelled the anatomical properties of a neuronal subpopulation of the Insular Cortex that belongs to a restricted network enrolling both bilateral dlBNST/CeA and contralateral Insula, mainly located in the layer II/III, expressing the molecular marker Satb2 and characterized by unmyelinated axons. Our findings enlightened the contribution of the Insula^{Ins} neurons in social preference only after 24 h of social isolation in male mice (Fig. 7). Selective genetic ablation of Insula^{Ins} neurons leads to a reduced interest in social stimulus after acute social isolation, which is a maladaptive behavior. Interestingly, our work revealed that Insula^{Ins} are more excitable after 24 h of social isolation compared to group-housed conditions. We highlight a shift in the calcium activity of Insula^{Ins} neurons in freely moving mice during social interaction only 24 h after social isolation. This Ins^{Ins} calcium activity shift might be key in the discrimination of the two stimuli in the three-chamber social test. This data suggests that alteration in Insula^{Ins} circuit created an imbalance in social homeostasis processes.

We identified that the Insular cortex received contralateral innervations from cortical regions by using a rAA2-retro-CAG-cre monosynaptic retrograde virus strategy in Ai9-dTomato mouse (Fig. 1a–f, Supplementary Fig 1g,h). We found that the majority of this contralateral cortical labeling was located in the contralateral Insular cortex while 14.08% of this labeling was in other contralateral heterotopic cortical regions (somatosensory, motor, and medial prefrontal cortical regions). Our experiments complete the extended characterization of the Insula whole brain mapping study focused on the ipsilateral brain side[41]. Despite we didn't quantify the ipsilateral retrograde labeling of Insula neurons in other cortical regions, since it was not our question, we did observe sparse retrograde labeling in these regions (data not shown). Quantification of this ipsilateral retrograde labeling

https://doi.org/10.1038/s41467-024-51389-4

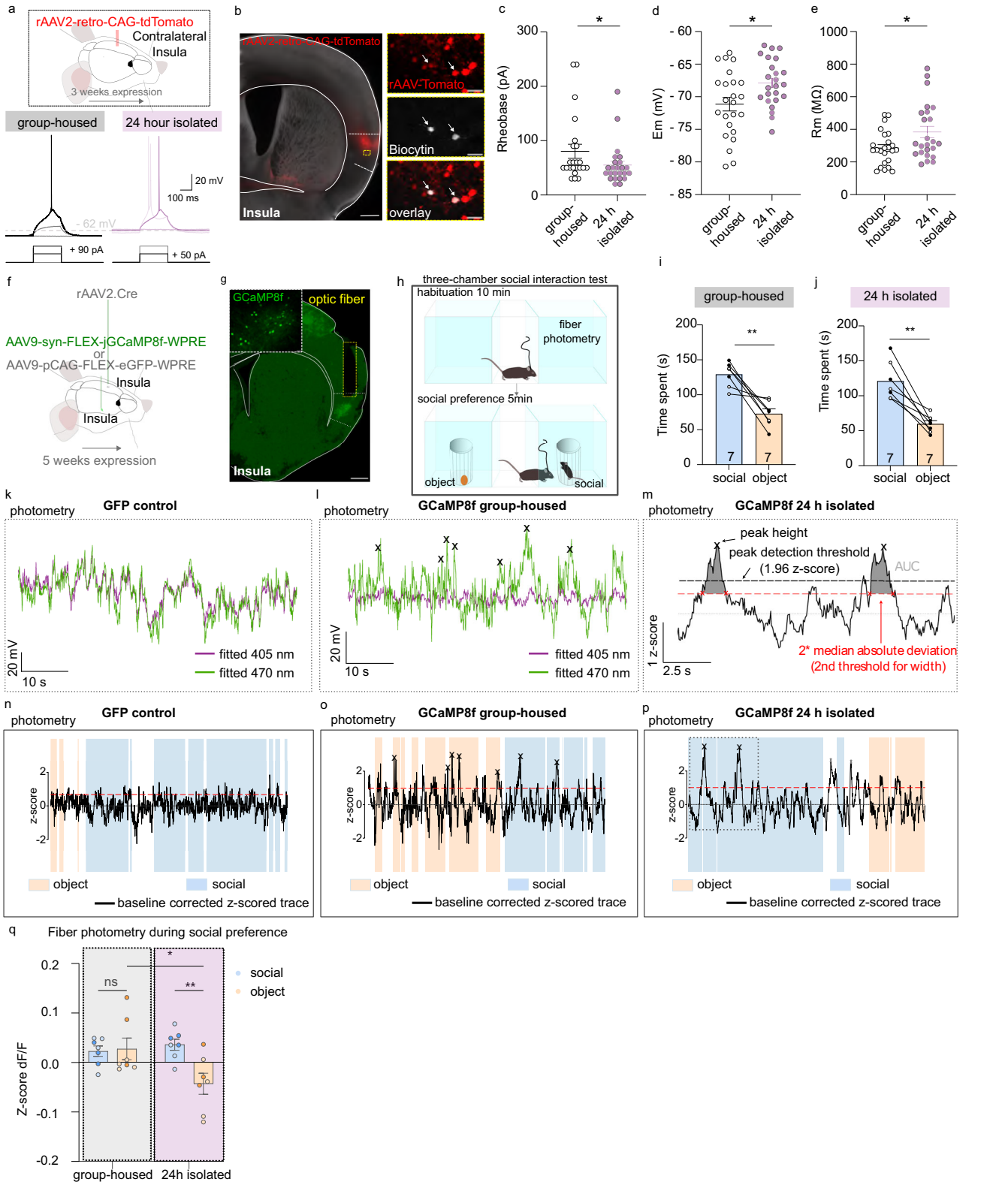

has been previously performed by using a rabies virus approach in CAMKII-cre mouse[41]. Potential differences in the quantity of ipsilateral retrograde labeling of Insula neurons in cortical regions may emerge between our studies. This potential discrepancy may account for distinct retrograde viral approaches used between studies.

In our study, we highlight that Ins^{Ins} neurons mainly project to the BNST, the CeA, the striatum, and the contralateral Insula by quantifying synaptophysin-eGFP puncta (Fig. 1g–i and Supplementary Fig. 2a, b). More specifically, we found that Ins^{Ins} neurons only project to the dorsolateral part of the BNST (juxtaBNST and the ovBNST), to the CeC and CeL, and the ventrodorsal part of the striatum with no projection to the dorsomedial, dorsolateral and neither to the tail of the striatum.

Pioneering studies including lesioning approaches and split-brain patient cases who presented surgical callosal incisions shed light on brain lateralized functions[42,43]. The degree of myelinization of axons

Fig. 6 | Impact of 24-hour social isolation on Insula^{Ins} neuronal activity. a Top. Experimental schematic. Bottom. Representative traces of Insula^{Ins} neurons in response to depolarizing current pulses (50 pA, 90 pA) in current clamp in group-housed and 24-hour isolated. **b** Representative example of a histological control showing Insula^{Ins} neurons (tomato) and Insula recorded neurons filled with biocytin (gray) and the overlay. **c**–**e** Group mean of the rheobase (**c**, Mann–Whitney test, $U = 183.5$, $p = 0.045$), resting membrane potential (**d**, two-tailed unpaired *t*-test, $t(46) = 2.549$, $p = 0.0142$), and resistance (e, Mann–Whitney test, $U = 190$, $p = 0.0437$) of Insula^{Ins} neurons in group-housed and 24-hour isolated mice (group-housed condition: 23 neurons in 3 mice; isolated conditions: 24 neurons in 3 mice). **f**, **h** Experimental schematic. **g** Representative epifluorescent image of a coronal brain slice injected with a rAAV2-Cre retrograde virus in the contralateral Insula, coupled with an AAV9-syn-flex-jCCaMP8f-WPRE virus injection in the ipsilateral Insula, along with the optic fiber placement. **i**, **j** Time spent around the juvenile social or the object enclosure in group-housed condition (**i**, two-tailed unpaired *t*-test, $t(6) = 4.682$, $p = 0.0034$) and after 24 h of social isolation (**j**, two-tailed unpaired *t*-test, $t(6) = 5.321$, $p = 0.0018$, white circle for female, black circle for male). **k**–**m** Example of fiber photometry recording in Insula^{Ins} neurons during three-chamber social interaction test in GFP control group (**k**, **n**), in GCaMP8f group-housed (**l**, **o**) and 24 h isolated mice (**m**, **p**). Blue and orange squares represent the episodes of interactions with the juvenile mouse or the object, respectively. Black arrows are the detected calcium events. **q** Quantification of ΔF/F mean fluorescence z-score of Insula^{Ins} neurons around social or object enclosure in both groups ($N = 7$ mice per group; two Way repeated measure Anova, Interaction $F(1,6) = 8.89$, $p = 0.0246$, main effect of housing $F(1,6) = 16.17$, $p = 0.007$, no main effect of zone $F(1,6) = 2.428$, $p = 0.1702$, followed by uncorrected Fisher's LSD post hoc, group-housed social vs group-housed object $p > 0.05$, 24 h isolated social vs object $p = 0.0073$, group-housed social vs 24 h isolated social $p > 0.05$, group-housed object vs 24 h isolated object $p = 0.012$). dark blue/orange color circle: female, light blue/orange color: male. Data are presented as mean values ± SEM. $^{*}p < 0.05$, $^{**}p < 0.01$.

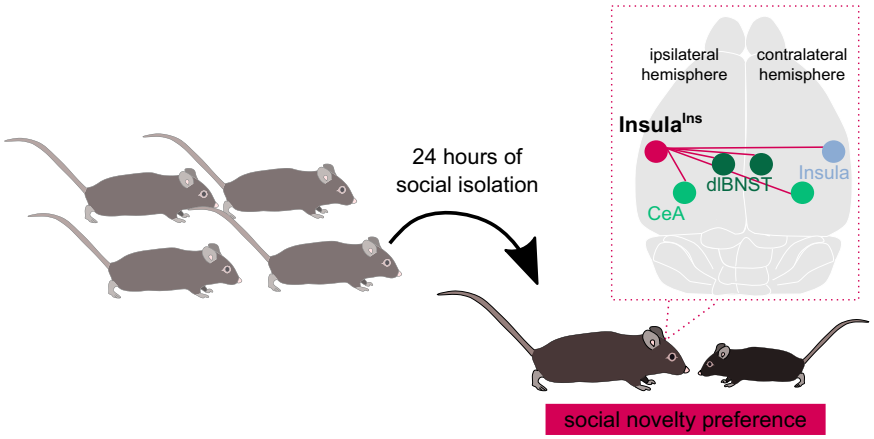

Fig. 7 | Summary schematic. Insula^{Ins} neurons are required for social novelty preference only after 24 h of social isolation in male mice.

directly impacts the efficiency of interhemispheric communication. Decreased efficiency in interhemispheric inhibition has been observed in children who are characterized by a hypo-myelination of callosal neurons resulting in difficulties in generating unilateral motor movement and leading to non-lateralized mirror movements[44]. The nature and the recruitment of cortical interhemispheric communication may depend on the type and the complexity of the performed task as well as the cortex involved[45]. Here, we found that stimulation of Insula^{Ins} neurons leads to excitation of the Insula contralateral side in mice (Fig. 3h–s).

In general, myelination of axons, which is a dynamic process, ensures a fast and precise transfer of information to the targeted zone. Thus, the degree of myelination is one of the parameters that influence the conduction velocity and define the efficiency of neuronal communication. Unexpectedly, the entire population of Ins^{Ins} are unmyelinated neurons in adult mice under physiological conditions (Fig. 2h, i). We confirmed this phenomenon by a low density in MBP immunostaining in the Insula (Fig. 2f) contrary to what has been described in other cortical regions[46,47]. This lack of myelination on Insula^{Ins} axons may explain the variability in their onset latency in response to axonal stimulation (Fig. 2e). Future studies would be required to understand this atypical Insula signature and the potential implication of myelination process within Insula^{Ins} neurons at synaptic, circuit and behavioral levels in physiological and pathological states.

In this study, we discovered that selective genetic ablation of Insula^{Ins} neurons impaired social preference only following acute social isolation (Fig. 4l–n). These results suggested a potential reduction in attention toward social stimuli and/or a lack of motivation to orient towards social cues when Insula^{Ins} neurons are lesioned after acute isolation. We did not detect a general deficit in motivation in Insula^{Ins} caspase mice (Supplementary Fig. 10). Together, these results suggest that Insula^{Ins} neurons may be activated when social homeostasis is disrupted, promoting adaptive and appropriately motivated behavior to seek social contacts. However, in our study, some experiments have been performed only in males or females. Further work should be assessed to evaluate the sex differences in motivational aspects and anxiety. Decreasing the excitability of Insula^{Ins} cells by using chemogenetic viral approach during the social interaction test was not sufficient to block the social preference after 24-h of social isolation as observed with the caspase strategy (Figs. 4 and 5). This data suggests that Insula^{Ins} neuron activation might rather occur during social isolation and be key for developing social preferences thereafter. We therefore show that Insula^{Ins} neurons are more depolarized and more excitable after 24 h of social isolation compared to group-housed mice (Fig. 6a–e). However, due to the technical limitations of chemogenetic approach and the other available viral tools, we were not able to block exclusively during the all 24 h isolation period the activity of Insula^{Ins} neurons, which remains an appealing question. Further studies should be done to investigate the effect of acute and long-lasting activation of this pathway on social behavior.

Here, by highlighting the complex axonal arborization of this Insular cortex subpopulation (Fig. 1 and Supplementary Fig. 2), we demonstrated that the subpopulation of Insular cortex neurons projecting to the insula/CeA/dlBNST network in both hemispheres holds a privileged position in controlling social behaviors in acute social isolation. Deciphering the relative contribution and adaptive plastic mechanisms occurring in each collateral target during 24 h of social isolation represents the next key step in a better understanding of social encoding process.

Interestingly, Insula^{Ins} neurons and dopaminergic neurons of the Dorsal Raphe Nucleus also project massively to the dlBNST and the CeA[34]. Future studies will be necessary to determine whether a specific neuronal target of Insula^{Ins} neurons is necessary to control social preference in isolation, or if, conversely, these neurons regulate social preference through coordinated action on the insula/BNST/CeA network, possibly in conjunction with dopamine modulation. Thus, all of these data suggest that Insula^{Ins} play a specific role in social interest. This specificity is confirmed as we did not observe an anxiety phenotype after Insula^{Ins} deletion, as assessed through an open field or an elevated plus maze. (Supplementary Fig. 8).

Here, we assessed a right unilateral lesion of Insula^{Ins} neurons by using a double viral approach (Fig. 4a). One limitation of our study is that our viral strategy may minimize the effect observed by manipulating a smaller quantity of cells. However, to be selective of Insula^{Ins} neurons without targeting interneurons (Supplementary Fig. 2d–f), we restricted our ablation to the right Insula^{Ins} neurons. Despite this limitation, our viral approach allowed a selective ablation of right Insula^{Ins} neurons which can be useful for future investigations of Insula lateralization. Indeed, lateralization of the Insula with a right dominance has been observed with cFos analysis in response to intraperitoneal injection of lithium chloride, an aversive visceral stimulus, or in feeding behavior[48,49]. Additional studies would be necessary to define the Insula laterization processes.

Our study, by demonstrating the role played by Insula^{Ins} neurons in social preference encoding during acute social isolation, reinforces the concept of cellular diversity of the Insula[28,29,38,47,49–52]. Another avenue for future research motivated by the present study will be to examine the development, maturation, and neuromodulation of this Insula^{Ins} circuit in physiological and pathological states where social processing is altered.

Methods

Experimental model and subject details

Animals. Male and female C57BL/6JRj (≥10 weeks; Elevage Janvier, France) were used. Male Ai9 tdTomato also called Gt(Rosa) 26Sortm6(CAG-tdTomato)Hze (stock number 007909, from Jackson; C57BL6/j genetic background) were also used. Mice were housed three to five per cage under controlled conditions (22–23 °C, 40% relative humidity, 12 h light/dark illumination cycle; with lights on at 07:00). Mice were acclimatized to laboratory conditions at least one week before experiments, with food and water *ad libidum*. All procedures were conducted following European directive 2010-63-EU and with approval from the Bordeaux University Animal Care and Use Committee (license authorization 21134).

Methods details

Viruses and drugs. rAAV2-retro-CAG-Cre ($2{,}8 \times 10^{12}$ vg/mL; UNC Vector Core, Boyden); rAAV2-retro-CAG-eYFP (1.6×10^{12} Virus Molecules/ml, UNC GTC Vector Core), rAAV2.-retro-CAG-tdTomato (3.6×10^{12} Virus Molecules/ml, UNC GTC Vector Core), AAV2.2-eif1a-DIO-eYFP (3×10^{12} vg/mL; Addgene); AAV2.5-eif1a-DIO-eYFP (1×10^{13} vg/mL; Addgene); AAV9-pCAG-FLEX-eGFP-WPRE (1×10^{13} vg/ml, 162379-AAV9, Addgene), AAV2.2-hSyn-eYFP (3×10^{12} vg/mL; 50465-AAV2, Addgene); AAV2.5−eif1a-DIO-eYFP (1×10^{13} vg/mL; 27056-AAV5, Addgene); AAV1-phSyn1(S)-FLEX_tdTomato-T2A-SypEGFP-WPRE (4.5×10^{12} vg/ml;51509-AAV, Addgene) AAV2.2-hSyn-ChR2(H134R)-eYFP (3.1×10^{12} vg/mL; UNC, AV4384G); AAV5-flex-taCasp3-TEVp (7×10^{12} vg/mL; Addgene); AAV9-syn-jGCaMp8f-WPRE (2.3×10^{13} vg/ml, 162379-AAV9, Addgene), AAV8-hSyn-DIO-HA-hM4D(GI)-IRES-mCitrine (1×10^{13} vg/ml, 50455-AAV8, Addgene), AAV5-hSyn-DIO-hM3D(Gq)-mCherry (2.5×10^{13}vg/ml, 4361-AAV5, Addgene), Tetrodotoxin (TTX, 0.5 μM, Abcam ab120055); and 4 aminopyridine (4AP; 1 mM, ascent scientific, asc-122-100mg).

Surgery. Stereotaxic surgery for anatomy, ex vivo and in vivo electrophysiology experiments, and behavioral tests were performed under a mixture of isoflurane and oxygen as previously described[53]. Mice were placed on a stereotaxic frame and received a subcutaneous dose of buprenorphine (0.1 mg/kg, except for in vivo electrophysiology experiments) and local injection of an analgesic before skin incision (lurocaine, 7 mg/kg). Single or bilateral craniotomy was made over the insular cortex at the following coordinates (+0.14 mm/bregma, ±3.8 mm/midline, 2.2 mm/brain surface), the CeA (−1.58 mm/bregma, +2.4 mm/midline, 3.9 mm/brain surface). Viruses were injected via a glass micropipette into the region of interest. Following injections, the incision was closed with sutures, and mice were let to wake up on a heating plate. For all the experiments the virus was incubated at least four weeks before proceeding with further manipulation except for the experiment with the retrograde virus (rAAV2-retro-CAG-cre) injection in AI9- dtTomato in which only two weeks were sufficient to clearly identify reporter protein expression.

Immunohistochemistry. Mice were deeply anesthetized with a mixture of isoflurane and oxygen and received an i.p. lethal dose of exagon (300 mg/kg) and lidocaine (30 mg/kg). Mice were perfused transcardially with phosphate-buffered saline (PBS 1X) and incubated (48 h/4 °C) in 4% paraformaldehyde. Coronal slices were cut at 50 μm and washed three times in PBS 1X before incubation in the blocking solution containing 0.03% Triton X-100 and 10% donkey serum or goat serum. Sections were incubated (overnight per 4 °C) with a mouse anti-Satb2 primary antibody (1/300; abcam ab51502), a rat anti-Ctip2 primary antibody (1/500; Abcam ab18465), or with a rat anti-MBP (1/500, Merckmillipore), a guinea pig anti-NeuN/Fox3 (1/1000, cat 26604, Synaptic system), or with a goat anti-CTb antibody (1/10000, list labs #703), or a rabbit anti-GFP primary antibody (1/1000; Millipore, AB3080), a mouse anti-GAD67 primary antibody (1/500; Millipore MAB5406), a guinea pig anti-PV primary antibody (1/1000, synaptic system, cat#195004). After washing sections were incubated overnight or 72 h for the CTb experiment at 4 °C with a donkey anti-mouse secondary antibody (labeling of Satb2, 1/500, life technologies A31571, Alexa 647), a donkey anti-rat secondary antibody (labeling of Ctip2 or labeling of MBP, 1/500, life technologies A21209, Alexa 488), a goat anti-mouse secondary antibody (labeling of GAD67,1/500, Invitrogen A21202, Alexa 488), a goat anti-guinea pig secondary antibody (labeling of PV or Neun/Fox3,1/500, Invitrogen A11073, Alexa 488), a donkey anti-goat 647 (labeling of CTb, 1/500, Jackson Immunoresearch, 705-605-147) a donkey anti-rabbit (labeling GFP,1/500, life technologies A21206, Alexa 488), streptavidin (labeling of biocytin, R&D system NL 999, 1/500, alexa 557). Sections were washed and then mounted in Fluoromont-G medium (Southern Biotech), coverslipped, and imaged on a fluorescent microscope as a confocal microscope (Leica SP5) or a slide scanner (Nanozomeer 2.0HT), or an epifluorescent microscope (Olympus BX63). Photomicrographs were taken and displayed using image J to adjust the contrast and or perform Z stack images.

Electron microscopy sample preparation

Tissue preparation. Mice were deeply anesthetized and perfused transcardially with a mixture of 3% paraformaldehyde (PFA) and 0.5% glutaraldehyde in 0.1 M phosphate buffer at pH 7.4. Brains were quickly removed, left overnight in 3% PFA at 4 °C. Coronal sections of the brain were cut on a vibrating microtome at 50 μm, collected in PBS, cryoprotected, freeze-thawed, and stored in PBS with 0.03% sodium azide until use.

Immunogold experiments. GFP was analyzed at electron microscopic level in Insula, Corpus Callosum, Anterior Commissure, dlBNST and CeA. GFP was detected by the preembedding immunogold technique, sections were incubated in 4% NGS for 45 min and then in a mixture of

a rabbit anti-GFP (1/5000) antibody supplemented with 1% NGS overnight at RT. After washing, in PBS and PBS-BSAc (aurion, the Netherlands), the sections were incubated for 3 h at RT in Goat anti-rabbit IgG conjugated to ultrasmall gold particles (1.4 nm; nanoprobes) diluted 1/100 in PBS-BSAc- gel. The sections were washed and post-fixed in 1% glutaraldehyde in PBS for 10 min. After washing in PBS and water distilled, the immunogold signal was intensified using a silver enhancement kit (HQ silver; Nanoprobes, Yaphank, NY) for 8 min at RT in the dark. After several washes in PBS, the sections were then processed for electron microscopy.

The sections were post-fixed in 0.5% osmium tetroxide and dehydrated in ascending series of ethanol dilutions that also included 70% ethanol containing 1% uranyl acetate. The sections were post-fixed, dehydrated, and included in resin (Durcupan ACM; Fluka). Serial ultrathin sections were cut with a Reichert Ultracut S, contrasted with lead citrate and imaged in a transmission electron microscope (H7650, Hitachi) equipped with a 467 SC1000 Orius camera (Gatan).

Ex vivo electrophysiology. After allowing at least 4 weeks for viral vector expression acute coronal brain slices containing the Insula were cut on a vibratome (VT1200S; Leica microsystems). Mice were deeply anaesthetized by i.p. injection of a mixture of ketamine-xylazine (100 mg/kg and 20 mg/Kg, respectively). A thoracotomy followed by a transcardiac perfusion with a saturated ($95\%O_2/5\%CO_2$), iced-cold solution (cutting solution) containing 250 mM sucrose,10 mM $MgSO_4{\cdot}7H_2O$, 2.5 mM KCl, 1.25 mM $NaH_2PO_4{\cdot}H_2O$, 0.5 mM $CaCl_2{\cdot}H_2O$, 1.3 mM $MgCl_2$, 26 mM $NaHCO_3$, and 10 mM D-glucose (pH 7.4) was performed. The brain was then quickly removed from the skull, blocked in the coronal plan, glued on the stage of the vibratome, submerged in iced-cold, saturated cutting solution and cut in 300-µm thick sections. Brain slices were transferred in a storage chamber at 34 °C for 1 h in an artificial cerebral spinal solution (referred as « recording ACSF ») saturated by bubbling $95\%O_2/5\%CO_2$ and containing 126 mM NaCl, 2.5 mM KCl, 1.25 mM $NaH_2PO_4{\cdot}H_2O$, 2 mM $CaCl_2{\cdot}H_2O$, 2 mM $MgSO_4{\cdot}7H_2O$, 26 mM $NaHCO_3$, and 10 mM D-glucose, supplemented with 5 mM glutathion and 1 mM sodium pyruvate (pH: 7.4; Osmolarity: 310-315 mOsm). They were then maintained at room temperature in the same solution until recording.

Whole-cell patch-clamp recordings were performed in a submerged chamber under an upright microscope (AxioExaminer Z1; Zeiss) equipped with IR-DIC illumination. Slices were bathed in recording solution. Recording pipettes (5–7 MΩ) were prepared from borosilicate glass capillaries (GC150F-10; Harvard Apparatus) with a horizontal puller (Sutter Instrument, Model P-97). They were filled an internal solution composed of 135 mM K-gluconate, 3.8 mM NaCl, 1 mM $MgCl_2{\cdot}6H_2O$,10 mM HEPES, 0.1 mM Na_4EGTA, 0.4 mM Na_2GTP, 2 mM $Mg_{1.5}ATP$, 5 mM QX-314 and 5 mM Biocytin (pH :7.25; Osmolarity: 290-295 mOsm). Experiments were conducted using a Multiclamp 700B amplifier and Digidata 1440 digitizer controlled by Clampex 10.6 (Molecular Devices) at 34 °C. Data were acquired at 20 kHz and low-pass filtered at 4 kHz. Insula pyramidal neurons were visualized under IR-DIC microscopy and recognized by the triangular shape of their soma. All the recordings were performed in voltage-clamp mode at −80 and 0 mV to record light-evoked glutamatergic EPSC and GABAergic IPSC, respectively. Voltages were corrected offline for liquid junction potentials. Optical stimulations were achieved using a 473 nm diode pumped solid state laser (Optotronics, USA) connected to an 800 µm diameter optical fiber (Errol, Paris, France) positioned just above the surface of the slice next to the recording site. Current clamp recordings were performed for the characterization of the intrinsic excitability of Insular neurons projecting to the tail of the striatum or the contralateral Insula in group-housed conditions and or after acute social isolation. For these experiments, internal solution was identical to the one used for voltage-clamp experiments but without QX-314.

At the end of the day, brain slices were fixed in 4% PFA overnight and stored in 0.2% sodium azide-PBS until histological processing.

In vivo electrophysiology. Electrical stimulation of the Insula. Bipolar electrical stimulation of the Insula was conducted with a concentric electrode (Phymep) and a stimulator isolator (800 µs, 0.2–1.8 mA; Digitimer).

Insula recordings. A glass micropipette filled with 2% pontamine sky blue solution in 0.5 M sodium acetate was lowered in the insula. The in vivo single-unit recordings were performed as previously described[54]. Briefly, the extracellular potential was recorded with an Axoclamp-2B amplifier and filter (300 Hz/0.5 kHz). Single neuron spikes were collected online (CED 1401, SPIKE 2; Cambridge Electronic Design). During electrical stimulation of one insula, cumulative peristimulus time histograms (PSTH) (5 ms bin width) of the contralateral Insula were generated for each neuron recorded. Electrical stimulation of the contralateral Insula was also used to test for antidromic activation of ipsilateral insula neurons using high-frequency stimulation and collision methods as previously described[55]. Driven impulses were considered antidromic if they met the following criteria: (1) constant latency of spike response (fixed jitter), (2) driven by each of the paired stimulus pulses at frequencies of 100 Hz or greater, and (3) collision of driven spikes by spontaneous impulses.

Histological control. At the end of each recording experiment, the recording pipette placement was marked with an iontophoretic deposit of pontamine sky blue dye (−20 µA; 30 min). To mark the electrical stimulation sites, +50 µA was passed through the stimulation electrode for 90 s. Then, mice were perfused with PBS 1x and stored for 48 h in PFA 4% at 4 °C.

Behavioral procedures. One week prior behavioral experiment, mice were progressively handled by the experimenter. For each behavioral test, mice were acclimatized at least 30 min in the experimental room. Between each mouse, the behavioral apparatus was cleaned with 70% ethanol and then water and dried between each test. For the chemogenetic behavioral experiment, a concentration of 1 mg/kg of Clozapine-N-Ozide (CNO) was administered intraperitoneally 30 min before the behavior.

Open field test. Mice were placed in the corner of a square open field (40 × 40 cm) and were allowed to freely explore the open field for a 10-min period in 70 lux illumination conditions. Total distance travelled, velocity, and time spent in the zone during the session were automatically reported (Ethovision, Noldus).

Elevated plus Maze. The elevated plus maze consisted of a platform of four opposite arms (30 cm × 5cm) two of them are open and two are closed arms (enclosed by 25 cm high walls). The apparatus was elevated from the floor. The task was analyzed with the software Ethovision (Noldus) and we measured the time spent in each arm in trials of 10 min. The luminosity of the open arms was around 120 lux.

Light-Dark box test. The apparatus is composed of two chambers of equal size (20 cm × 20 cm each), a light compartment (between 575 and 600 lux), and a dark compartment (between 5 and 25 lux). Mice were placed in the same corner in the dark compartment. The session lasted 15 min and was scored with the software Ethovision (Noldus, Wageningen, the Netherlands).

Marble burying test. Mice are placed in a corner of a new open arena (37.5 cm × 37.5 cm, 200 lux). filled with a thin layer of wood chip bedding and covered on the surface by twenty 1.4 cm diameter black marbles organized in 5 rows and 4 columns The mice were free to explore for 20 min. The number of totally buried marbles was counted using Image J.

Novelty-suppressed feeding behavior. Mice are food-deprived and isolated for 24 h and then tested for latency to eat a chow in a novel open arena for a maximum period of 5 min. Immediately after the first bite, mice were transferred to her home cage with a chow. The latency to the first bite in a chow was manually scored.

Social preference test. A three-chamber rectangular Plexiglas arena (60x42x22 cm, Imetronic) divided into three chambers of the same dimension was used for this test. Briefly, each mouse was placed in the center of the arena and allowed to freely explore the entire arena for a 10 min habituation period under approximately 90 lux illumination conditions. At the end of the habituation, the mouse was placed in the center of the arena, and two metallic enclosures (9 cm × 9 cm x 10 cm) were positioned in the center of the two outer chambers. One enclosure contained a juvenile unfamiliar mouse, whereas the other enclosure was empty (inanimate object) for group-housed conditions or filled with Lego toys for isolated conditions. The position of the two enclosures was counterbalanced to avoid any bias. The juvenile mice were previously habituated to the enclosure and the arena for a brief period of 2 days preceding the experiment with a 10-min session per day. The experimental mouse was allowed to freely explore the three-chamber arena for a 5 min period session. The time spent around the enclosures were manually scored. The stimulus interaction was scored when the nose of the experimental mouse was in closed proximity to the enclosure (approximatively around 2 cm).

Oral self-administration

Apparatus and general procedure. As described elsewhere[56], mice were trained in conditioning chambers (15x18x22cm, Imetronic, France), each located inside a sound and light-attenuating wooden chamber. Each experimental chamber had an operant panel equipped with two nose-poke holes and a liquid dipper was inserted in between. External pumps were fitted with syringes connected with Tygon tubing to a fluid dispenser. A microcomputer controlled the delivery of liquid rewards, presentation of cue light, and recording of behavioral data (Imetronic, France).

The illumination of a dim house-light for 3 s signaled the start of each test session. Visits in the "active" hole resulted in a 50µl-liquid reward delivered into the dipper, accompanied by the presentation of a visual stimulus consisting of a 3 s cue light above the active nose-poke. After each delivery, mice had to empty the liquid dispenser to enable the next count of reinforced visits. Visits to the inactive hole were recorded but had no consequences. At the end of the training session, the illumination of the house-light again signaled the termination of the session.

training. Female Mice were trained to nose-poke for a liquid reward of sweet condensed milk (scm, Regilait®) on a fixed ratio schedule of reinforcement: FR1 for 4 days, FR2 for 4 days, and FR5 for 3 days on a daily 30 min-session to acquire efficient instrumental response prior the motivation test. There were two groups compared: control ($n = 6$) and caspase ($n = 6$).

Motivation. Mice were tested for the motivation for sweet condensed milk in a progressive ratio schedule of reinforcement. Within the same session, the number of visits in the active nose-poke hole to obtain the reward increased progressively by 2 (PR2). The session lasted 120 min and we applied a cut-off after 15 min without a reward delivery. The breaking point, which is the operational index of motivation, was calculated on the last ratio a mouse completed before the session was stopped. A first PR2 test was performed after the last FR2 session, then a second one was performed after the last FR5 session. Experiments were done blindly.

Fiber photometry. 4 male mice and 3 female mice were injected with 100 nL of rAAV2-retro-CAG-cre in the contralateral insular cortex (left hemisphere). Mice were then injected with either 60 nL of pGP-AAV9-syn-FLEX-jGCaMP8f-WPRE in the ipsilateral insular cortex (right hemisphere). The optic fiber (Doric lenses, 400 µm, 0.57NA, 4 mm) was implanted 300 µm above the injection site in the right insular cortex to record the calcium events in the cell bodies. Optic fiber efficiency was tested beforehand and was used if reached a minimum of 90% efficiency. Recordings started five weeks after the stereotaxic surgeries to allow for viral expression of the GCaMP sensor. Mice were handled 10 min for 5 days before the start of the experiments and habituated to being connected to the optic fiber after the 3rd day of handling.

The bulk fluorescence activity of $Insula^{Ins}$ neurons was recorded via the expression of the GCaMP sensor 8 f with Doric fiber photometry systems. Light was transmitted to the optic fiber through two light emitting diodes, using alternated emission at 20 Hz of the 405 nm and 470 nm wavelength. The 473 nm LED was used to record activity changes, and the 405 nm LED was used as our control signal, to remove unrelated signal artifacts (such as motion artifacts) as this isosbestic wavelength is calcium-independent. The LEDs were coupled to optical fiber patch cords (400 µm, NA: 0.57), which were connected to the optical fiber ferrules (400 µm, NA: 0.57). At the beginning of recording sessions, the power of the LED was adjusted to have at the tip of the optic fiber: For the 470 nm LED: 100 µW, for the 405 nm: 25–30 µW. This was re-adjusted and lowered for GFP controls to record a non-saturated signal. To synchronize the video with the fiber photometry recordings, the camera was externally triggered by uEye Cockpit software which emitted a TTL for each frame to the Doric Neuroscience Studio. Camera recordings were done at 30 fps, at 512 × 512 resolution. For all animals and behavioral assay, recordings started at least two minutes before the start of experiment for photobleaching the signal. The position of the mouse and key positions of the apparatus and objects were determined using the open-source software DeepLabCut 2.0[57,58]. The tracking of the head was used for the analysis.

The normalized *dF/F (z dF/F)*, was calculated as described ref. 59. All analysis was done using custom scripts on Python.

(1) Low-frequency fluctuations and signal drift were removed using the adaptive iteratively reweighted Penalized Least Squares (airPLS) algorithm () on the 405 nm control signal and 470 nm calcium-dependent signal.

(2) Each signal was standardized (z-scored). $z\ signal = \frac{signal - mean(signal)}{std(signal)}$

(3) A least-squares linear fit was applied to the 405 nm control signal and fitted to the 470 nm signal over the whole behavioral recording. This signal was then subtracted from the z-scored 470 nm signal:

$$z\Delta F/F = [z470nm\ signal - fitted(z405nm)]$$

To determine the average activity within the regions of interest (ROI), we averaged the z-scored trace when the animals for each frame within the ROI (global signal). The last five minutes of habituation and first five minutes in the behavioral apparatus was used.

Peaks were detected if above 1.96 on the z-scored trace with a minimum distance between peaks of 500 ms and duration of 150 ms. The start and end of the peak were calculated based on when the signal crossed 2*Median Absolute Deviation (MAD). The Area Under the Curve (AUC) was calculated between those two points using the trapezoidal rule. The width was calculated as the time between those two points. The height corresponds to the z-score value at peak detection.

We performed an alternated analysis to compute and compare the z-scored trace as described in refs. 60,61 ref. The fractional $\Delta F/F$, a least-squares linear fit was applied to the 405 nm control signal and fitted to the 473 nm signal over the whole behavioral recording

($\Delta F/F$ = ([473 nm signal − 405 nm fitted]/405 nm fitted). The ΔF/F were then z-scored over the entire behavioral session.

Data analysis

For in vivo electrophysiological experiments, cumulative PSTHs of insula activity were generated during stimulation of the contralateral insula. Excitatory magnitudes were normalized for different levels of baseline impulse activity. Baseline activity was calculated on each PSTH, during the 500 ms preceding the stimulation to generate a *Z*-score for each responding neuron. What is referred to as a "no response cell" is a neuron that does not emit an action potential in response to stimulation of the insula, specifically within the time window ranging from 0 to 25 ms after stimulation. Baseline activity was computed for each peri-stimulus time histogram (PSTH) during the 500 ms preceding stimulation to generate a Z-score for each responsive neuron. A "no response cell" is a neuron with a Z-score <1.96, meaning a probability value (p) > 0.05 of emitting an action potential within the time window of a monosynaptic transmission between the ipsilateral and contralateral insula (i.e., between 0 and 25 ms).

For immunolabeling quantification. To quantify retrograde labeling (rAAV2-retro-CAG-cre/Ai9dtomato mouse), we acquired 3 slices for each Insula level (antero, intermediate and posterior level) per mouse, on a total of 4 mice with a confocal microscope. For the co-localization of Tomato$^+$ neurons with Satb2$^+$ and Ctip2$^+$ labeling, we took 3 pictures with a confocal microscope per slice, on 3 slices per mouse, with a total of 4 mice and analyzed co-localization on focal plan manually with Image J cell counter. For the caspase lesion, we took one picture in the mid-Insula level with a slide scanner per mouse and quantified with Image J, the fluorescence density between the contralateral (ctrl side) and ipsilateral lesion side (caspase side).

For the CTb quantification experiment, we used semi-automatic quantification with an Image J macro for co-localization of fluorescent markers present on a focal plan on confocal fluorescent images called Bioloc3D. More information is available at this link https://zenodo.org/doi/10.5281/zenodo.8087692.

Synaptophysin imaging and analysis

Confocal imaging over one focal place was done on the whole slice (with a map of Z planes across the slice to avoid confounds) at x20 magnification using confocal microscopy (Zeiss, Celldiscoverer 7). Slices were then semi-automatically aligned to the Allen Brain Atlas CCFv3 using QuPath[62] and Aligning Big Brains and Atlases Fiji plugin Fiji. Synaptophysin puncta were detected using the QuPath Positive Cell Detection tool. To avoid artifact detections, we excluded single puncta in a 20 μm area. For each brain structure in the slice, the sum of the area of Synaptophysin puncta was calculated. Ipsilateral Insula (GU/VISC/AI) was systematically removed from the quantification (presence of cell bodies). We then manually delimited subregions in the Bed Nucleus of the Stria terminalis (oval, juxta-capsular, anteromedial, and ventral), Central Amygdala (lateral–capsular and medial), and Dorsal Striatum (Dorsomedial, Dorsolateral, Ventral and Tail of Striatum). The density was calculated as the sum of the area of Synaptophysin puncta/area. To normalize between mice, all the results are expressed as a percentage of the total.

Statistical analysis

Statistical outliers were identified with the Grubbs test and excluded from the analysis. Normality was checked with the Shapiro-Wilk criterion and when violated, non-parametric statistics were applied (Mann–Whitney and Kruskal–Wallis, Wilcoxon test). When samples were normally distributed, data were analyzed with independent or paired one or two-tailed samples *t*-tests, one-way, two-way, or repeated measures ANOVA followed if significant by Bonferroni *post hoc* tests or with uncorrected Fisher's LSD. Data are represented as the mean ± SEM, and the significance was set at $p < 0.05$. Data were analyzed using GraphPad Prism 9.

Reporting summary

Further information on research design is available in the Nature Portfolio Reporting Summary linked to this article.

Data availability

None Source data are provided with this paper.

References

1. Gogolla, N., Takesian, A. E., Feng, G., Fagiolini, M. & Hensch, T. K. Sensory integration in mouse insular cortex reflects GABA circuit maturation. *Neuron* **83**, 894–905 (2014).
2. Salomon, R. et al. The insula mediates access to awareness of visual stimuli presented synchronously to the heartbeat. *J. Neurosci.* **36**, 5115–5127 (2016).
3. Miura, I. et al. Encoding of social exploration by neural ensembles in the insular cortex. *PLoS Biol.* **18**, e3000584 (2020).
4. Bird, C. W. et al. Ifenprodil infusion in agranular insular cortex alters social behavior and vocalizations in rats exposed to moderate levels of ethanol during prenatal development. *Behav. Brain Res.* **320**, 1–11 (2017).
5. Cavalcante, L. E. S. et al. Modulation of the storage of social recognition memory by neurotransmitter systems in the insular cortex. *Behav. Brain Res.* **334**, 129–134 (2017).
6. Ramos-Prats, A. et al. VIP-expressing interneurons in the anterior insular cortex contribute to sensory processing to regulate adaptive behavior. *Cell Rep.* **39**, 110893 (2022).
7. Rieger, N. S. et al. Insular cortex corticotropin-releasing factor integrates stress signaling with social affective behavior. *Neuropsychopharmacology* **47**, 1156–1168 (2022).
8. Rogers-Carter, M. M., Djerdjaj, A., Gribbons, K. B., Varela, J. A. & Christianson, J. P. Insular cortex projections to nucleus accumbens core mediate social approach to stressed juvenile rats. *J. Neurosci.* **39**, 8717–8729 (2019).
9. Rogers-Carter, M. M. & Christianson, J. P. An insular view of the social decision-making network. *Neurosci. Biobehav. Rev.* **103**, 119–132 (2019).
10. Alvarez, R. P. et al. Increased anterior insula activity in anxious individuals is linked to diminished perceived control. *Transl. Psychiatry* **5**, e591–e591 (2015).
11. Terasawa, Y., Shibata, M., Moriguchi, Y. & Umeda, S. Anterior insular cortex mediates bodily sensibility and social anxiety. *Soc. Cogn. Affect Neurosci.* **8**, 259–266 (2013).
12. Odriozola, P. et al. Insula response and connectivity during social and non-social attention in children with autism. *Soc. Cogn. Affect Neurosci.* **11**, 433–444 (2016).
13. Uddin, L. Q. & Menon, V. The anterior insula in autism: Underconnected and under-examined. *Neurosci. Biobehav. Rev.* **33**, 1198–1203 (2009).
14. Etkin, A., Prater, K. E., Schatzberg, A. F., Menon, V. & Greicius, M. D. Disrupted amygdalar subregion functional connectivity and evidence of a compensatory network in generalized anxiety disorder. *Arch. Gen. Psychiatry* **66**, 1361–1372 (2009).
15. Gogolla, N. The insular cortex. *Curr. Biol.* **27**, R580–R586 (2017).
16. Zhang, Z. & Oppenheimer, S. M. Electrophysiological evidence for reciprocal insulo-insular connectivity of baroreceptor-related neurons. *Brain Res.* **863**, 25–41 (2000).
17. Yao, S., Becker, B. & Kendrick, K. M. Reduced inter-hemispheric resting state functional connectivity and its association with social deficits in autism. *Front. Psychiatry* **12**, 629870 (2021).
18. Anderson, J. S. et al. Decreased interhemispheric functional connectivity in autism. *Cereb. Cortex* **21**, 1134–1146 (2011).

19. Linke, A. C., Jao Keehn, R. J., Pueschel, E. B., Fishman, I. & Müller, R.-A. Children with ASD show links between aberrant sound processing, social symptoms, and atypical auditory interhemispheric and thalamocortical functional connectivity. *Dev. Cogn. Neurosci.* **29**, 117–126 (2018).
20. Bocchi, R. et al. Perturbed Wnt signaling leads to neuronal migration delay, altered interhemispheric connections and impaired social behavior. *Nat. Commun.* **8**, 1158 (2017).
21. Compton, R. J. et al. Trouble crossing the bridge: altered interhemispheric communication of emotional images in anxiety. *Emotion* **8**, 684–692 (2008).
22. Suárez, R. et al. A pan-mammalian map of interhemispheric brain connections predates the evolution of the corpus callosum. *Proc. Natl Acad. Sci. USA* **115**, 9622–9627 (2018).
23. Takeuchi, N., Oouchida, Y. & Izumi, S.-I. Motor control and neural plasticity through interhemispheric interactions. *Neural Plast.* **2012**, 823285 (2012).
24. Domínguez-Iturza, N. et al. The autism- and schizophrenia-associated protein CYFIP1 regulates bilateral brain connectivity and behaviour. *Nat. Commun.* **10**, 3454 (2019).
25. Harb, K. et al. Area-specific development of distinct projection neuron subclasses is regulated by postnatal epigenetic modifications. *Elife* **5**, e09531 (2016).
26. Schiff, H. C. et al. An insula-central amygdala circuit for guiding tastant-reinforced choice behavior. *J. Neurosci.* **38**, 1418–1429 (2018).
27. Ponserre, M., Peters, C., Fermani, F., Conzelmann, K.-K. & Klein, R. The insula cortex contacts distinct output streams of the central amygdala. *J. Neurosci.* **40**, 8870–8882 (2020).
28. Zhang-Molina, C., Schmit, M. B. & Cai, H. Neural circuit mechanism underlying the feeding controlled by insula-central amygdala pathway. *iScience* **23**,101033 (2020).
29. Luchsinger, J. R. et al. Delineation of an insula-BNST circuit engaged by struggling behavior that regulates avoidance in mice. *Nat. Commun.* **12**, 3561 (2021).
30. Bastide, M. F. et al. Involvement of the bed nucleus of the stria terminalis in L-Dopa induced dyskinesia. *Sci. Rep.* **7**, 2348 (2017).
31. Geffen, G. M., Jones, D. L. & Geffen, L. B. Interhemispheric control of manual motor activity. *Behav. Brain Res.* **64**, 131–140 (1994).
32. Bloom, J. S. & Hynd, G. W. The role of the corpus callosum in interhemispheric transfer of information: excitation or inhibition? *Neuropsychol. Rev.* **15**, 59–71 (2005).
33. van der Knaap, L. J. & van der Ham, I. J. M. How does the corpus callosum mediate interhemispheric transfer? A review. *Behav. Brain Res.* **223**, 211–221 (2011).
34. Matthews, G. A. et al. Dorsal raphe dopamine neurons represent the experience of social isolation. *Cell* **164**, 617–631 (2016).
35. Conrad, K. L., Louderback, K. M., Gessner, C. P. & Winder, D. G. Stress-induced alterations in anxiety-like behavior and adaptations in plasticity in the bed nucleus of the stria terminalis. *Physiol. Behav.* **104**, 248–256 (2011).
36. Somerville, L. H., Whalen, P. J. & Kelley, W. M. Human bed nucleus of the stria terminalis indexes hypervigilant threat monitoring. *Biol. Psychiatry* **68**, 416–424 (2010).
37. Mobbs, D. et al. Neural activity associated with monitoring the oscillating threat value of a tarantula. *Proc. Natl Acad. Sci. USA* **107**, 20582–20586 (2010).
38. Gehrlach, D. A. et al. Aversive state processing in the posterior insular cortex. *Nat. Neurosci.* **22**, 1424–1437 (2019).
39. Méndez-Ruette, M. et al. The role of the rodent insula in anxiety. *Front. Physiol.* **10**, 330 (2019).
40. Shi, T., Feng, S., Wei, M. & Zhou, W. Role of the anterior agranular insular cortex in the modulation of fear and anxiety. *Brain Res. Bull.* **155**, 174–183 (2020).
41. Gehrlach, D. A. et al. A whole-brain connectivity map of mouse insular cortex. *eLife* **9**, e55585 (2020).
42. Wolman, D. The split brain: a tale of two halves. *Nature* **483**, 260 (2012).
43. Ortigue, S., King, D., Gazzaniga, M., Miller, M. & Grafton, S. Right hemisphere dominance for understanding the intentions of others: evidence from a split-brain patient. *Case Rep.* **2009**, bcr072008 0593 (2009).
44. Beaulé, V., Tremblay, S. & Théoret, H. Interhemispheric control of unilateral movement. *Neural Plast.* **2012**, 627816 (2012).
45. Stark, D. E. et al. Regional variation in interhemispheric coordination of intrinsic hemodynamic fluctuations. *J. Neurosci.* **28**, 13754–13764 (2008).
46. Call, C. L. & Bergles, D. E. Cortical neurons exhibit diverse myelination patterns that scale between mouse brain regions and regenerate after demyelination. *Nat. Commun.* **12**, 4767 (2021).
47. Grady, F., Peltekian, L., Iverson, G. & Geerling, J. C. Direct parabrachial–cortical connectivity. *Cereb. Cortex* **30**, 4811–4833 (2020).
48. Qian, K., Liu, J., Cao, Y., Yang, J. & Qiu, S. Intraperitoneal injection of lithium chloride induces lateralized activation of the insular cortex in adult mice. *Mol. Brain* **14**, 71 (2021).
49. Wu, Y. et al. The anterior insular cortex unilaterally controls feeding in response to aversive visceral stimuli in mice. *Nat. Commun.* **11**, 640 (2020).
50. Kayyal, H. et al. Insula to mPFC reciprocal connectivity differentially underlies novel taste neophobic response and learning in mice. *eLife* **10**, e66686 (2021).
51. Kayyal, H. et al. Activity of insula to basolateral amygdala projecting neurons is necessary and sufficient for taste valence representation. *J. Neurosci.* **39**, 9369–9382 (2019).
52. Ju, A., Fernandez-Arroyo, B., Wu, Y., Jacky, D. & Beyeler, A. Expression of serotonin 1A and 2A receptors in molecular- and projection-defined neurons of the mouse insular cortex. *Mol. Brain* **13**, 99 (2020).
53. Glangetas, C. et al. NMDA-receptor-dependent plasticity in the bed nucleus of the stria terminalis triggers long-term anxiolysis. *Nat. Commun.* **8**, 14456 (2017).
54. Glangetas, C. et al. Ventral subiculum stimulation promotes persistent hyperactivity of dopamine neurons and facilitates behavioral effects of cocaine. *Cell Rep.* **13**, 2287–2296 (2015).
55. Georges, F. & Aston-Jones, G. Activation of ventral tegmental area cells by the bed nucleus of the stria terminalis: a novel excitatory amino acid input to midbrain dopamine neurons. *J. Neurosci.* **22**, 5173–5187 (2002).
56. Tannous, S., Darlot, F., Cador, M. & Caille, S. Flavor additives facilitate oral self-administration of nicotine solution in mice. *Psychopharmacology* **238**, 2235–2247 (2021).
57. Mathis, A. et al. DeepLabCut: markerless pose estimation of user-defined body parts with deep learning. *Nat. Neurosci.* **21**, 1281–1289 (2018).
58. Nath, T. et al. Using DeepLabCut for 3D markerless pose estimation across species and behaviors. *Nat. Protoc.* **14**, 2152–2176 (2019).
59. Martianova, E., Aronson, S. & Proulx, C. D. Multi-fiber photometry to record neural activity in freely-moving animals. *J. Vis. Exp.* https://doi.org/10.3791/60278 (2019)
60. Lerner, T. N. et al. Intact-brain analyses reveal distinct information carried by SNc dopamine subcircuits. *Cell* **162**, 635–647 (2015).
61. Morel, C. et al. Midbrain projection to the basolateral amygdala encodes anxiety-like but not depression-like behaviors. *Nat. Commun.* **13**, 1532 (2022).
62. Bankhead, P. et al. QuPath: open source software for digital pathology image analysis. *Sci. Rep.* **7**, 16878 (2017).

Acknowledgements
C.G. is supported by the Foundation for Medical Research: ARF20170938746. This work was supported by recurrent funding from the University of Bordeaux and the CNRS. This study also received financial support from the French government in the framework of the University of Bordeaux's IdEx "Investments for the Future" program / GPR BRAIN_2030. The microscopy was done in the Bordeaux Imaging Center a service unit of the CNRS-INSERM and Bordeaux University, member of the national infrastructure France BioImaging supported by the French National Research Agency (ANR-10-INBS-04). The help of Sebastien Marais is acknowledged.

Author contributions
C.G. and F.G. conceived and designed the experiments. C.G. performed and analyzed the anatomical study with the participation of E.L., M.G., T.D., M.L., E.D., and E.B. performed the data with electron microscopy. C.G. and A.G. performed and analyzed the in vivo electrophysiology in anesthetized mice. L.B., A.T., and J.B. designed, performed, and analyzed the ex vivo electrophysiological experiments. C.G. and A.G. performed and analyzed the behavioral study. S.C. tested and analyzed the motivation for sweet food in mice. A.B. performed the fiber photometry experiment and A.B. and C.G. analyzed it. C.G. and F.G. wrote the manuscript and C.G. prepared the figures.

Competing interests
The authors declare no competing interests.

Additional information
Supplementary information The online version contains supplementary material available at https://doi.org/10.1038/s41467-024-51389-4.

Correspondence and requests for materials should be addressed to Christelle Glangetas or François Georges.

Peer review information *Nature Communications* thanks Nadine Gogolla, Francesco Papaleo and the other, anonymous, reviewer(s) for their contribution to the peer review of this work. A peer review file is available.